博士論文

Pathophysiological analyses of cortical malformation using gyrencephalic mammals.

（脳回をもつ動物を用いた大脳皮質形成異常の病態生理学的解析）

桝田　宏輔

博士論文

Pathophysiological analyses of cortical malformation using gyrencephalic mammals.

(脳回をもつ動物を用いた 大脳皮質形成異常の病態生理学的解析)

脳神経医学専攻・神経内科学

指導教員

辻 省次 先生

申請者

桝田 宏輔

Table of Contents

Abstract

One of the most prominent features of the cerebral cortex of higher mammals is the presence of gyri and sulci. Because malformations of the cortical gyri are associated with severe disability in brain function, the mechanisms underlying malformations of the cortical gyri have been of great interest. However, the brain of mice does not have the cortical gyri, it is therefore difficult to investigate the mechanisms of malformations of the cortical gyri using mice. Combining gyrencephalic carnivore ferrets and genetic manipulations using *in utero* electroporation, here I successfully recapitulated the cortical phenotypes of thanatophoric dysplasia (TD) by expressing fibroblast growth factor 8 (FGF8) in the ferret cerebral cortex. Interestingly, in contrast to TD model mice reported in previous studies, FGF8-transfected ferrets showed not only megalencephaly but also polymicrogyria and periventricular nodular heterotopia, which were observed in human TD patients. I further uncovered that neural progenitors such as outer radial glial cells (oRGs) and intermediate progenitor cells (IPs) were markedly increased in the developing cerebral cortex of FGF8-transfected ferrets. Because it has been proposed that increased oRGs and/or IPs resulted in the appearance of cortical gyri during evolution, it seemed reasonable to speculate that increased oRGs and IPs underlie the pathogenesis of polymicrogyria. My findings using FGF8-transfected ferrets should be helpful for clarifying the molecular mechanisms underlying the development and malformation of cortical gyri and sulci in higher mammals.

Introduction

Abnormal corticogenesis in humans

The cerebral cortex is crucial for higher brain functions and is especially developed in higher mammals including humans. One of the prominent features of the cerebral cortex of higher mammals is the presence of gyri and sulci. Humans, monkeys and ferrets have gyrencephalic brains (i.e. brains with a folded cerebral cortex), while the brains of rodents are often lissencephalic (i.e. lacking cortical folds). Because malformations of the cortical gyri and sulci during development are associated with severe disability in brain function and diseases such as lissencephaly, polymicrogyria, periventricular nodular heterotopia, epilepsy, schizophrenia and autism[1-7], the mechanisms underlying the development and malformation of the cortical gyri and sulci have been of great interest.

Polymicrogyria refers to a malformation of cortical gyrification, which is composed of too many abnormal small gyri and sulci (Fig 1a). Because polymicrogyria is associated with various causes, such as congenital infections (particularly cytomegalovirus infection), localized or diffuse ischemia during the fetal period, and several genetic syndromes (for example, Aicardi syndrome, Delleman syndrome, DiGeorge syndrome), the appearance of polymicrogyria in macroscopic and microscopic observations varies depending on the causes. Polymicrogyria may be found unilaterally (~40%) or bilaterally (~60%), and focally or diffusely. The most frequent site of polymicrogyria is around the sylvian fissure (~80%), and the others are the frontal lobe (~70%), the parietal lobe (~65%), the temporal lobe (~40%), and the occipital lobe (~10%). Polymicrogyria is often associated with general cortical malformations, such as corpus callosum agenesis, cerebellar hypoplasia, periventricular

nodular heterotopia, subcortical heterotopia, and macrocephaly. Previous histological studies reported that polymicrogyria had various layer patterns of the cerebral cortex, such as an unlayered polymicrogyria and a 4-layered polymicrogyria. The main symptoms of polymicrogyria are hemiparesis, cognitive dysfunction and epilepsy [4,5,8-17].

Periventricular nodular heterotopia (PNH) is histologically recognized as neuronal nodules closed to the lateral ventricle (Fig. 1b). PNH is caused by abnormal migration of neurons and is observed in about 30% of malformations of cortical development. Common clinical presentations of PNH are seizures and learning difficulties. Although genetic mutations related to PNH are not fully understood, the most common mutation is observed in filamin 1 gene (FLNA) in Xq28, and PNH caused by FLNA mutation exhibits X-linked dominant inheritance [5,18,19]. Recent studies showed that overactivation of the PI3K-AKT signaling pathway, which is one of downstream pathways of FGF receptor 3, leads to PNH in human [20] and in NEDD4L mutant mice [21].

Thanatophoric dysplasia and FGF receptor 3

Thanatophoric dysplasia (TD) exhibits polymicorgyria. TD is a lethal chondrodysplastic dwarfism, which is relatively common skeletal dysplasia [22,23]. The incidence of TD is 1:20,000 – 1: 50,000 births, and patients of TD decease within a few days after birth. TD has two main phenotypes, which are skeletal malformations and brain malformations. The skeletal malformations of TD patients can be traditionally divided into two groups (TD type 1 and TD type 2); TD type 1 has the curved femurs and craniosynostosis, whereas TD type 2 has the straight femurs and the cloverleaf skull.

The brain malformations of TD patients include megalencephaly, polymicrogyria, periventricular nodular heterotopia and hydrocephalus. Both TD type 1 and TD type 2 are caused by mutations in the FGF receptor 3 (FGFR3) gene located on 4p16.3 [24-31]. These mutations lead to constitutive activation of FGFR3 [32,33]. However, the relationship between the constitutive activation of FGFR3 and the cortical malformation is still ambiguous [22].

It was reported that TD type 2 has a point mutation substituting the amino acid lysine 650 for glutamic acid (K650E). Iwata et al. generated K644E (corresponding to K650E in human) mutant mice, whose FGFR3 was activated constitutively all over the body (K644E-all mice or TD mice). As well as TD type 2 human patients, K644E-all mice died soon after birth, so that postnatal cortical neurogenesis could not be analyzed. Lin et al. generated K644E mutant mice whose FGFR3 was activated constitutively only in the central nervous system (K644E-CNS mice or TD-CNS mice) by using the Cre/loxp system. K644E-CNS mice survived after birth, and their brains displayed megalencephaly, whereas the abnormal gyrification (i.e. polymicrogyria) was not observed. Further investigation of K644E-CNS mice revealed the increase of cortical thickness, the increase of intermediate progenitor cells (IPCs) and the decrease of an apoptosis during the early stage of neurogenesis. Meanwhile, K644E-CNS mice did not show the increase of radial glial cells and the change of cortical areal patterning. Because TD-CNS mice did not show polymicrogyria, which is found in human TD type 2[34-38], it is impossible to investigate the pathogenesis of polymicrogyria of TD using mice.

To examine the mechanisms of the formation and malformation of cortical gyri and sulci in higher mammals, Hiroshi Kawasaki (Kanazawa University, Ishikawa,

Japan) has utilized gyrencephalic carnivore ferrets, which have been widely used for neuroscientific research[39-42]. For example, neural progenitors in the outer subventricular zone have been charactrized using ferrets as described below [43,44]. However, genetic manipulation techniques for the ferret brain have rarely been reported previously. Therefore, to manipulate gene expression in the ferret cerebral cortex, Hiroshi Kawasaki recently established a rapid and efficient gene manipulation technique for ferret using *in utero* electroporation as described below [45,46].

Differences of the developing cerebral cortex in rodents and primates

In the developing cerebral cortex, neural stem cells exist in the ventricular zone (VZ) (Fig. 2). Neural stem cells, also known as radial glial cells (RGs), have bipolar morphology and contact with both the ventricular (apical) and pial (basal) surfaces of the neocortex[47,48]. In early stages of neurogenesis, RGs divide symmetrically and replicate. As neurogenesis progresses, RGs divide asymmetrically and produce RGs (self-renewal) and daughter progenitor cells (intermediate progenitor cells, IPs) in the subventricular zone (SVZ). One IP usually undergoes one symmetric division and produces two neurons[49,50]. The majority of neurons are produced by IPs during all stages[51]. Corticogenesis of primates is featured by the appearance of a large SVZ that has an inner (ISVZ) and outer region (OSVZ) compared with that of rodents [52-55]. In addition to RGs and IPs of the developing cortex in rodents, oRGs in the OSVZ are present in the developing cortex in primates. oRGs are unipolar, with basal fibers that ascend toward the pia but without apical fibers that descend toward the ventricle, while RGs in the VZ are bipolar [56,57]. Large neocortex tends to have the thicker OSVZ and

much more oRGs. It has been hypothesized that regions with more and less amounts of SVZ proliferation would predict the future locations of gyri and sulci, respectively [58]. Regions of the future gyri contain more proliferating cells in the OSVZ during development than those of the future sulci [43].

In utero electroporation for mice and ferrets

Electroporation began to be used in order to transfer genes into chicken embryos since 1997[59-61]. Electroporation was applied to the mouse brain in 2001, and modifications of procedures were needed because mouse embryos develop in the uterus[62-64]. This procedure called *in utero* electroporation consists of plasmid injection into the ventricle of embryos within the uterus and application of electric pulses to embryos. *In utero* electroporation has several advantages as follows; 1) easy to perform, 2) high transfection efficiency, 3) localized and unilateral transfer of genes, 4) co-transfection of multiple genes into one cell, 5) long-term expression of transfected genes. Other conditions of *in utero* electroporation for mice had already established; 1) 0.1-1 mg/ml total plasmid concentration, 2) electroporation pulse of 50 V, 50 ms, 5 times at 1 second intervals[62].

I*n utero* electroporation procedures for mice were not suitable for ferrets because the uterine wall of ferrets was thicker than that of mice. The first modification was the usage of transmitted light for illuminating the ferret embryo because the thicker uterine wall resulted in the concealment of the position of the embryo. By using transmitted light, the location of the iris of the ferret embryo became visible and indicated the position of the lateral ventricle. The second modification was the usage of higher voltages (100-150 V) for ferrets. Higher voltages led to higher expression levels, but

also to lower survival rates (50 V 100%, 100 V 85%, 150 V 65%). Owing to the several modifications for ferrets, Hiroshi Kawasaki (Kanazawa University, Ishikawa, Japan) recently established a rapid and efficient gene manipulation technique for ferrets using *in utero* electroporation to manipulate gene expression in the ferret cerebral cortex[45,46].

The role of FGFs and FGF receptors in the developmental brain

There are 22 types of fibroblast growth factors (FGFs) in the human genome, and many of them play various important roles in the developmental brain [37,65,66]. FGF1 and FGF2 regulate proliferation and survival of neuroepithelial cells. FGF2-null mice showed that both cortical neurons and glial cells were reduced[67]. FGF3 and FGF10 are related to inner ear development, and FGF3 knockout mice showed inner ear defects[68,69]. As well as FGF17 and FGF18, FGF8 is expressed in the midline region of the anterior neural ridge (ANR) and the midbrain-hindbrain boundary (MHB), and regulates the regionalization of neural primordium. FGF8 is broadly and strongly expressed in ANR and MHB at E8.5 in mice, but the expression of FGF8 gradually reduces by E15.5 [70,71]. FGF9 regulates the initiation of astrogenesis. FGF9 increased Olig2-positive cells, which are known as immature glial progenitor cells, in mouse forebrain slices in vitro at E16.5[72].

FGF receptors (FGFRs) have three immunoglobulin-like (Ig) domains in the extracellular region and two tyrosine kinase domains in the intracellular region. FGFRs are consisted of 4 subtypes, FGFR1-4, encoded on four different genes. Furthermore, FGFR1-3 have splicing in the Ig domains, which results in receptor isoforms of class b

and c (for example, FGFR1b and 1c). Different types of FGFRs have different affinities to various FGFs. The dimerization of FGFRs by FGFs leads to autophosphorylation of the intracellular region of FGFRs. Downstream signaling pathways of FGFRs include multiple pathways. One is the mitogen-activated protein kinase (MAPK) pathway, which regulates cell proliferation. Other pathways include the PI3K-AKT pathway and the PLC γ -PKC pathway [37,66,73].

My strategy to recapitulate polymicrogyria

As discussed above, TD-CNS mice did not show polymicrogyria, and it is therefore impossible to investigate the pathogenesis of polymicrogyria of TD using mice. This is presumably because mice do not have gyri and sulci on the cerebral cortex. To examine the mechanisms of the formation and malformation of cortical gyri and sulci in higher mammals, Hiroshi Kawasaki recently established a rapid and efficient gene manipulation technique for ferret using *in utero* electroporation[45,46].

Using *in utero* electroporation technique for ferrets, I decided to make polymicrogyria. To stimulate FGFR3 in the developing ferret cortex, I chose to express mouse FGF8b because FGF8b has the highest affinity to FGFR3 and because the amino acid sequence of mouse FGF8b is highly homologous to that of ferret FGF8 excluding some amino acids in the N-terminal helix of FGF8b which is not related to binding to FGFRs. The FGFR binding site of FGF8b is known as the β -trefoil core, which is composed of β 1- β 12 loops[74,75]. The amino acid sequence of the β 1- β 12 loops is the same completely between mouse FGF8b and ferret FGF8. Therefore, I speculated that mouse FGF8b works in the ferret cortex. Here I successfully recapitulated

polymicrogyria by overexpressing mouse FGF8b in the ferret cerebral cortex, and investigated the pathophysiology of polymicrogyria.

Materials and Methods

Animals.

Normally pigmented, sable ferrets (*Mustela putorius furo*) were purchased from Marshall Farms (North Rose, NY). Ferrets were bred as described previously[39-41]. Postnatal day 0 (P0) was defined as the day of birth. All procedures were performed in accordance with protocols approved by the Animal Care Committee of Kanazawa University. Experiments were repeated at least three times and gave consistent results.

The developmental processes of the ferret cortex have been reported previously. At embryonic day 30 (E30), the ferret cortex has a large germinal layer, where the neural stem cells (radial glia) exist. Then, 5 layers, the ventricular zone (VZ), the subventricular zone (SVZ), the intermediate zone (IZ), the cortical plate (CP) and the marginal zone (MZ), are gradually produced. At E38, the SVZ is divided into the outer SVZ (OSVZ) and the inner SVZ (ISVZ) by the inner fiber layer (IFL). At E42/P0, ferret babies are usually born. 2/3 layer in the cerebral cortex is formed around P6, which roughly corresponds to P3 in mice, and the neurogenesis in the cerebral cortex is almost completed at P14. Ferrets become mature at P48 [43,44].

In utero electroporation for ferrets.

In utero electroporation using ferrets was performed by Dr. Hiroshi Kawasaki (Kanazawa University, Ishikawa, Japan) as described above and previously[45,46]. Briefly, pregnant ferrets were deeply anesthetized, and their body was warmed using a heating pad to keep their body temperature. The uterine horns were exposed, and the embryo was visualized with light delivered through an optical fiber cable. Based on the location of the pigmented iris, the position of the lateral ventricle was identified.

Approximately 2–5 μl of DNA solution was injected into either the right or left lateral ventricle using a pulled glass micropipette. Each head of an embryo within the uterus was placed between tweezer-type electrodes with a diameter of 5 mm (CUY650-P5, NEPA Gene, Japan). The anode of the electrodes was placed on the cortex of the injected side so that the cortex of the injection side was transfected. Square electric pulses (100V, 50ms) were passed 5 times at 1-second intervals using an electroporator (ECM830, Harvard Apparatus, MA). The wall of the abdominal cavity and the skin were sutured, and the embryos were allowed to develop normally in the uterus of their mother.

Two kinds of plasmid mixtures were used per one pregnant ferret mother. The babies transfected with different genes were distinguished by the position (i.e. right or left cortex) of the GFP fluorescence. In this study, FGF8b plasmid mixture was injected into the right cerebral cortex, and control plasmid mixture into the left cortex. The ferret brains were harvested at P6, P16, and P36. About 50% of electroporated ferret babies survived until the day of sampling. The expression of transfected GFP was observed at least until P36. The numbers of brain samples were written below. FGF8; P6, n=3; P16, n=5; P36, n=8. Control; P6, n=6; P16, n=6; P36, n=11.

Plasmids.

pCAG-GFP was a generous gift from Dr. Tetsuichiro Saito (Chiba University, Chiba, Japan) and described previously (Fig. 3a)[76]. Briefly, pCAG-GFP was produced by inserting the GFP DNA fragment into pCAG vector using *EcoRI*. To make pCAG-FGF8b, the DNA fragment of mouse FGF8b was purchased from the DNAFORM (Kanagawa, Japan), and was inserted into pCAG vector using *EcoRI* (Fig.

3b). The plasmid sequences of pCAG-GFP and pCAG-FGF8b were confirmed. Plasmids were purified using an Endofree Plasmid Maxi kit (Qiagen, Germany). Prior to *in utero* electroporation experiments, plasmid DNA was diluted to 1–3 mg/ml in PBS, and Fast Green solution was added at a final concentration of 0.5% to confirm whether the plasmid mixture was injected in the lateral ventricle or not.

Immunohistochemistry.

Immunohistochemistry was performed as described previously with slight modifications[77-79]. Briefly, ferrets were deeply anesthetized and transcardially perfused with 4% paraformaldehyde (PFA)/PBS. After the brain was dissected, the brain was cryoprotected by being immersed in 30% sucrose for 3 days and embedded in OCT compound. Coronal sections (50 μ m) were made using a cryostat from the anterior part of the brains. At the beginning, sections containing the frontal lobe appeared. After the anterior part of the lateral ventricle became visible, the third ventricle emerged. Sections containing the anterior part of the lateral ventricle without the third ventricle were used for further analyses. The sections were obtained at least almost 20-30 slices per pup at each age. The sections were permeabilized with 0.5% Triton X-100/PBS and incubated overnight with primary antibodies, which included anti-Ki-67 antibody (Leica), anti-phospho-histone H3 (pH3) antibody (Upstate Biotechnology), anti-pH3 antibody (Millipore), biotin-conjugated anti-pH3 antibody (Millipore), anti-Olig2 antibody (Immuno-Biological Laboratories, Japan), anti-Pax6 antibody (Abcam), anti-Pax6 antibody (Covance), anti-phosphorylated vimentin (pVim) antibody (Medical & Biological Laboratories, Japan), anti-Tbr2 antibody (Abcam), anti-NeuN antibody (Chemicon), anti-GFAP antibody (Sigma-Aldrich), anti-APC

antibody (Calbiochem), anti-Brn2 antibody (Santa Cruz Biotechnology), anti-Ctip2 antibody (Abcam) and anti-FOXP2 antibody (Abcam). After being incubated with secondary antibodies and Hoechst 33342, the sections were washed and mounted on glass slides. Experiments were repeated at least three times and gave consistent results.

***In situ* hybridization.**

In situ hybridization was performed by Dr. Yohei Shinmyo (Kanazawa University, Ishikawa, Japan). Sections prepared from fresh-frozen tissues or fixed tissues were treated with prehybridization buffer (4% paraformaldehyde for 10 min, 1 μg/ml proteinase K for 10 min and 0.25% acetic anhydride) for 10 min. After prehybridization, the sections were incubated overnight at 58°C with digoxigenin-labeled RNA probes in hybridization buffer (50% formamide, 5× SSC, 5× Denhardt's solution, 0.3 mg/ml yeast RNA, 0.1mg/ml herring sperm DNA, and 1mM DTT). Next, the sections were incubated with alkaline phosphatase-conjugated anti-digoxigenin antibody (Roche, Indianapolis, IN). Finally the sections were incubated with NBT/BCIP. Experiments were repeated at least three times in different animals and gave consistent results.

Microscopy.

Epifluorescence microscopy was performed with an AxioImager A1 microscope (Carl Zeiss) or a BIOREVO BZ-9000 (Keyence). Confocal microscopy was performed with an FV10i FLUOVIEW microscope (OLYMPUS).

Cell counting.

Confocal microscopic images were acquired using an FV10i FLUOVIEW microscope (OLYMPUS). The numbers of Hoechst 33342-positive cells were counted automatically using Metamorph software. The numbers of immunopositive cells were manually counted using the "cell counter" function of ImageJ software, and were divided by the numbers of Hoechst 33342-positive cells.

Quantification of cortical folding.

Serial coronal sections with 50μm thickness were prepared, and sections containing the anterior part of the lateral ventricle were used for further analyses. After staining with Hoechst 33342, images were acquired using a BZ-9000 microscope (Keyence).

The gyrification index (GI) was calculated as described previously (Fig. 4)[80]. Briefly, the length of the complete contour and that of the outer contour of the electroporated side of the cortical hemisphere were measured. The ratio of the lengths of these two contours was calculated as follows.

The GI value = the length of the complete contour/the length of the outer contour

I newly defined the gyrification number index (GN), which indicates how many times the pial surface was detached from the outer contour of the brain (Fig. 5). Then the GN values of the transfected side (GNt) were divided by those of the other control side (GNo). The resultant GNt/GNo values would be 1 if the numbers of cortical folds were the same between the manipulated side and the control side of the cerebral cortex. The GNt/GNo values would be larger than 1 if the numbers of cortical folds in the manipulated side were larger than those in the control side.

Quantification of the sizes of the brain and the lateral ventricle.

Coronal sections containing the anterior part of the lateral ventricle were used for quantification. The area within the complete contour (see Fig. 4, green line) of either the transfected side or the other side of the brain was measured using ImageJ software. To minimize the variation of the size depending on the position of coronal sections, I calculated the ratio of the size of the transfected side and that of the other side. The ratio would be 1 if the size of the transfected side was the same as that of the other side, and would be larger than 1 if the size of the transfected side was larger than that of the other side. Similarly, the size of the lateral ventricle was measured. The area of the lateral ventricle of either the transfected side or the other side of the brain was measured using ImageJ software, and the ratio of the size of the transfected side and that of the other side was calculated.

Quantification of the average thickness of cortical layers.

Coronal sections containing the anterior part of the lateral ventricle obtained at P36 were used for quantification. To calculate the average thickness of layers 2/3, 4 and 5/6 around the coronal sulcus, the area of each layer was measured over a length of at least 5 mm and was subsequently divided by the length of each layer. Layers were identified using Brn2, Ctip2 and FoxP2 immunostaining and Hoechst 33342 staining.

Quantification of the GFAP-positive area.

Coronal sections containing the anterior part of the lateral ventricle obtained at P36 were stained with anti-GFAP antibody and Hoechst 33342, and were used for quantification (Fig. 5). The region of the cortical hemisphere located dorsal to the corpus callosum was selected because the GFP-positive cells were mainly located in

this region, and the selection excluded the cortical surface (Fig. 6, broken line). The area within the broken line and the area containing GFAP signals within the broken line were measured using ImageJ software, and the latter was divided by the former.

Statistical analyses.

Statistical analyses were performed using Statcel3 software (OMS Publishing, Japan) and *XL*STAT software (Addinsoft, Japan). After the *F*-test was performed, the *p* values were determined using a Student's *t*-test or a Welch's *t*-test. Kolmogorov-Smirnov test was also used. Bonfferoni correction was used for multiple comparisons. "n" means the number of animals.

Results

FGF8 induces cortical malformation in the ferret cerebral cortex

To make cortical phenotypes of TD, I expressed FGF8 in the cerebral cortex of gyrencephalic ferrets because FGFR3, which is responsible for TD patients, is preferentially activated by FGF8[81,82]. *In utero* electroporation was performed to express mouse FGF8 and GFP in the cerebral cortex of ferret embryos at E33, which roughly corresponds to E13 in mice, as described previously[45,46]. To detect the distribution patterns of ectopically expressed mouse *FGF8* mRNA selectively, *in situ* hybridization with a mouse FGF8 probe using the transfected ferret cerebral cortex was performed. As expected, mouse *FGF8* mRNA was indeed expressed in GFP-positive cells (Fig. 7), suggesting that the distribution patterns of GFP-positive cells represent those of ectopically expressed *FGF8* mRNA.

After electroporation was performed at E33, brain samples were obtained at P6, when cortical gyri have not yet been formed; at P16, when they are starting to form; and at P36, when they have been formed[83]. In control ferrets, the cortical surface was smooth, and the cortical gyrus was not evident at P6 (Fig. 8a, control). Consistent with previous studies[83], cortical gyri were visible at P16, and became more prominent at P36 (Fig. 8a, control). Cortical sulci such as the coronal sulcus and the suprasylvian sulcus were clearly visible. Importantly, there were no apparent differences in the patterns of cortical gyri between the GFP-electroporated side and the other side in control ferrets (Fig. 8a, control), suggesting that genetic manipulation using *in utero* electroporation does not have obvious adverse effects on gyrification.

Interestingly, I found that the FGF8-transfected cortex had more complicated gyrus patterns than the GFP-transfected control cortex at P16 (Fig. 8a, arrow). While

sulci and gyri that existed on the control brain were similarly distributed on the FGF8-transfected cortex, a number of undulating folds were added where FGF8 was expressed. Newly added folds became more prominent at P36 (Fig. 8a,b, arrows). These results suggest that the FGF8-transfected cortex shows polymicrogyria, which is one of the most common phenotypes of TD patients[22,23]. In addition to the patterns of cortical folding, the brain of the FGF8-electroporated side was larger than that of the other side (Fig. 8a). Quantification of brain sizes showed that the FGF8-transfected hemisphere tended to be larger than the GFP-transfected control hemisphere at P6 (control, 29.101 ± 0.423 mm^2; FGF8, 32.092 ± 1.614 mm^2; Student's *t*-test; p=0.065), P16 (control, 61.237 ± 1.920 mm^2; FGF8, 68.140 ± 3.0711 mm^2; Student's *t*-test; p=0.054) and P36 (control, 105.932 ± 5.858 mm^2; FGF8, 125.015 ± 12.785 mm^2; Student's *t*-test; p=0.127). Because the measured values of brain sizes were influenced by the positions of sections, the ratio of the size of the transfected hemisphere to that of the non-transfected hemisphere on the same section was calculated. The ratio of brain sizes showed that the FGF8-transfected hemisphere was significantly larger than the GFP-transfected control hemisphere at P6 (control, 1.023 ± 0.029; FGF8, 1.245 ± 0.063; Student's *t*-test; $p < 0.05$), P16 (control, 0.967 ± 0.015; FGF8, 1.104±0.028; Student's *t*-test; $p<0.01$) and P36 (control, 0.981±0.014; FGF8, 1.327±0.091; Welch's *t*-test; $p<0.05$) (Fig. 9a–c). This is consistent with the fact that megalencephaly is a common phenotype of TD patients[22]. The size of the lateral ventricle was also measured, and the result showed that the lateral ventricle in the FGF8-transfected hemisphere was significantly larger than that in the GFP-transfected control hemisphere at P6 (control, 2.083 ± 0.951 mm^2; FGF8, 5.714 ± 1.178 mm^2; Student's *t*-test; $p<0.05$), P16 (control, 0.744 ± 0.326 mm^2; FGF8, 2.897 ± 0.485 mm^2; Student's *t*-test; $p<0.01$) and P36 (control, 1.417 ± 1.068

mm^2; FGF8, 6.948 ± 3.420 mm^2; Student's *t*-test; p=0.094). As in the case of brain sizes, the ratio of the size of the lateral ventricle of the transfected side to that of the non-transfected side on the same section was calculated. This ratio showed that the lateral ventricle of the FGF8-transfected hemisphere was significantly larger than that of the GFP-transfected control hemisphere at P6 (control, 1.02 ± 0.17; FGF8, 3.63 ± 0.61; Student's *t*-test; $p < 0.01$), P16 (control, 0.83 ± 0.20; FGF8, 2.82 ± 0.88; Student's *t*-test; $p < 0.05$) and P36 (control, 1.02 ± 0.42; FGF8, 4.37 ± 0.51; Student's *t*-test; $p < 0.01$) (Fig. 9d–f and Fig. 10a). The enlargement of the lateral ventricle could contribute to megalencephaly.

Interestingly, although FGF8-electroporated ferrets exhibited polymicrogyria, it was reported that polymicrogyria was not found in TD-CNS mice [34,35]. This could be because ferrets have gyrencephalic brains, and therefore ferrets seemed to be more appropriate for investigating the mechanisms of cortical malformation than mice. These findings suggest that FGF8-transfected ferrets are useful for examining the pathophysiology of polymicrogyria in the brain.

Characterization of cortical folding in FGF8-electroporated ferrets

I quantified the effect of FGF8 on cortical folding using coronal sections. Coronal sections containing the anterior part of the lateral ventricle were used for further analyses. Consistent with my macroscopic observations (Fig. 8), coronal sections showed increased cortical folds in the FGF8-electroporated cortex compared with the GFP-electroporated control cortex at P36 (Fig. 10, asterisks).

I measured the length of the complete contour (i.e. the pial surface) and that of the outer contour of the brain using coronal sections, and calculated the gyrification

index (GI), which is the ratio of the length of the complete contour to that of the outer contour (See the Materials and Methods section and Fig. 4 for details)[80]. The GI values would be 1 if there were no cortical folds, and would become larger numbers if cortical folds were formed. Indeed, the GI values were almost 1 at P6, when cortical folds were not evident, and became larger thereafter in control ferrets as cortical gyri appeared (P16, 1.32±0.03; P36, 1.55±0.04; Student's *t*-test, $p<0.01$) (Fig. 11a,b). Consistent with my macroscopic observations (Fig. 8), I found that the GI values were significantly larger in the FGF8-electroporated ferret brain than in the control brain at P36 (control, 1.55 ± 0.04; FGF8, 1.72 ± 0.04; Student's *t*-test, $p < 0.05$) (Fig. 11b). These results suggest that FGF8 induces ectopic cortical folds. Although my macroscopic observations found polymicrogyria as early as P16 (Fig. 8), the GI values did not show significant differences between FGF8-electroporated and control ferrets at P16 (control, 1.32 ± 0.03; FGF8, 1.28 ± 0.07; Student's *t*-test, $p > 0.05$) (Fig. 11a). This discrepancy could be due to two possible reasons. The first possibility was newly formed sulci were not deep enough to be detected by the GI values at P16 and became deep enough to be detected at P36. The second possibility was that the cortical folding was affected only locally where FGF8 was transfected (Fig. 10a, arrows). Because the GI values reflect cortical folding of the entire contour of the brain (Fig. 4), it seemed possible that the GI values were not sensitive enough to detect the changes in shallows and local cortical folding.

The larger GI values in FGF8-electroporated ferrets could result from two possible reasons. The first possible reason would be that the number of cortical folds was larger in the FGF8-electroporated ferret brain. The second possibility is that the depth of cortical sulci became deeper in the FGF8-electroporated ferret brain. To

distinguish these possibilities, I newly defined the gyrification number index (GN), which indicates how many times the pial surface is detached from the outer contour of the brain (See the Materials and Methods section and Fig. 5 for details). Then the GN values from the transfected side of the cortex (GNt) were divided by those from the other side of the cortex (GNo) in the same brain sections. The GNt/GNo values would be 1 if the numbers of cortical folds were the same between the transfected side and the other side, and would be larger than 1 if the number of cortical folds was increased on the transfected side. Consistent with the GI values, I found that the GNt/GNo values were significantly larger at P36 (control, 0.94 ± 0.08; FGF8, 1.43 ± 0.05; Student's *t*-test; $p < 0.01$) (Fig. 11d). This finding clearly indicates the number of cortical folds is increased in FGF8-electroporated ferrets. Furthermore, in contrast to the GI values, the GNt/GNo values were significantly larger not only at P36 but also at P16 (control, 1.08 ± 0.12; FGF8, 1.58 ± 0.12; Student's *t*-test, $p < 0.05$) (Fig. 11c). The GNt/GNo values seem to increase earlier and/or to be sensitive in the developmental steps to detect abnormalities in cortical folding than the GI values.

Because it seemed possible that FGF8 electroporated into one side of the brain also affected gyrification on the other side, I examined the GI values of the hemisphere contralateral to the FGF8-electroporated side at P36. The GI values of the hemisphere contralateral to the FGF8-electroporated side at P36 were indistinguishable from those of the GFP-electroporated control brain (control, 1.55 ± 0.04; FGF8, 1.59 ± 0.03; Student's *t*-test, $p > 0.05$). This result suggests that FGF8 electroporation on one side of the brain does not have apparent effects on gyrification on the other side.

Histological changes of the cerebral cortex in developing FGF8-electroporated ferrets

I examined histological changes of the cerebral cortex at P6 using coronal sections stained with Hoechst 33342 (Fig. 12a). In the developing cortex of gyrencephalic mammals, there are mainly three types of proliferating cells: RGs, IPs and oRGs [84-90]. RGs (known as apical RGs/ventricular RGs/apical progenitors) are epithelial stem cells in the VZ and generate IPs (also known as basal progenitors) that migrate into the SVZ. Corticogenesis in higher mammals is distinguished by the presence of the large SVZ, which is often divided by the inner fiber layer (IFL) into an inner (ISVZ) and outer region (OSVZ) [53,54]. oRGs (also known as OSVZ RGs/basal RGs/intermediate RGs/translocating RGs) are a recently identified novel class of progenitor cells that are abundant in the OSVZ of the developmental cortex in gyrencephalic mammals. Interestingly, I found that the ISVZ and the OSVZ were markedly thicker and contained much more Hoechst-positive cells in the developing cortex of FGF8-electroporated ferrets than in control ferrets at P6 (control, 7961.6 ± 677.4 cells/mm^2; FGF8, 12317.6 ± 930.8 cells/mm^2; Student's *t*-test; $p<0.01$) (Fig. 12a). Because the ISVZ and the OSVZ contain proliferating cells such as oRGs and IPs, these results raised the possibility that cell proliferation is enhanced in FGF8-electroporated ferrets.

To examine if cell proliferation is enhanced in the GFP-positive electroporated cortical area of FGF8-electroporated ferrets (Fig. 8a, arrowheads), I performed immunohistochemistry using anti-Ki-67 antibody and anti-phospho-histone H3 (pH3) antibody at P6. I found that the numbers of Ki-67-positive cells and pH3-positive cells were prominently increased in the FGF8-electroporated cortex at P6 (Fig. 12b,c), suggesting that cell proliferation is indeed enhanced in

FGF8-electroporated ferrets. Many Ki-67-positive cells and pH3-positive cells were predominantly distributed in the ISVZ and the OSVZ, where neural progenitors are dividing. Interestingly, I also found a large number of Ki-67-positive cells and pH3-positive cells in the intermediate zone (IZ) and the cortical plate (CP) of the FGF8-electroporated ferret cortex, where dividing cells are rarely found in the normal ferret cortex [44]. This result suggests that cell proliferation is also enhanced in the IZ and the CP.

I further examined the percentages of proliferating cells. The numbers of Ki-67-positive cells were counted and divided by those of Hoechst-positive cells. The percentages of Ki-67-positive proliferating cells were more than double in the cerebral cortex of FGF8-electroporated ferrets (control, 5.1±0.6%; FGF8, 11.9±1.1%; Student's *t*-test, $p < 0.01$) (Fig. 13a). Interestingly, the percentages of Ki-67-positive cells in FGF8-electroporated ferrets were significantly higher in the OSVZ (control, 7.3±1.2%; FGF8, 13.3±1.5%; Student's *t*-test, $p<0.05$), in the ISVZ (control, 9.7±1.3%; FGF8, 14.5±1.3%; Student's *t*-test, $p<0.05$) and in the IZ/CP (control, 1.3±0.10%; FGF8, 9.7±1.0%; Welch's *t*-test, $p<0.01$) (Fig. 13b,c). Consistent results were obtained with pH3 staining. The percentages of pH3-positive cells were 4-fold higher in the cerebral cortex of FGF8-electroporated ferrets (control, 0.18±0.07%; FGF8, 0.80±0.09%; Student's *t*-test, $p<0.01$) (Fig. 13d). The percentages of pH3-positive cells in FGF8-electroporated ferrets were significantly higher in the OSVZ (control, 0.25±0.16%; FGF8, 0.72±0.14%; Student's *t*-test, $p<0.05$), in the ISVZ (control, 0.30±0.09%; FGF8, 0.79±0.18%; Student's *t*-test, $p<0.05$) and in the IZ/CP (control, 0.035±0.025%; FGF8, 0.80±0.23%; Welch's *t*-test, $p<0.05$) (Fig. 13e,f). These results clearly indicate that cell proliferation in the OSVZ and the ISVZ is stimulated.

Because the border between the VZ and the SVZ was often difficult to define in the cerebral cortex of FGF8-electroporated ferrets, I also counted Ki-67- and pH3-positive cells using a more objective definition of regions of interest (ROI). I divided the cortex into 10 regions along the radial axis from the ventricular surface to the pial surface (Fig. 14a), and quantified Ki-67- and pH3-positive cells in each region. The percentages of Ki-67- and pH3-positive cells were significantly larger in upper regions of the FGF8-transfected cortex than those of the GFP-transfected control cortex after Bonfferoni correction (Fig. 14b,c), suggesting that cell proliferation is enhanced in the cerebral cortex of FGF8-electroporated ferrets, especially in the upper cortical regions. Consistently, Kolmogorov-Smirnov test showed that the percentages of pH3-positive cells were significantly larger in the FGF8-transfected cortex than those of the GFP-transfected control cortex ($p<0.0001$).

It should be noted that the locations of GFP-positive transfected cells and those whose proliferation had increased were spatially distinct. GFP-positive cells were located in the CP of the cerebral cortex, whereas increased Ki-67- and pH3-positive cells were distributed not only in the CP but also in the IZ and the SVZ (Fig. 12b,c). These results suggest that FGF8 exerts its effects on dividing cells that are in locations distinct from those of GFP-positive somata in the cerebral cortex. FGF8 could diffuse easily in the cortical tissues to exert its effects. Alternatively, FGF8 could be released from GFP-positive axons located close to dividing cells. Consistently, *in situ* hybridization showed that FGF receptors such as *FGFR2* and *FGFR3* were expressed in the VZ and the SVZ of the ferret cerebral cortex at E40 (Fig. 15). These expression patterns are consistent with a recent report showing the expression patterns of FGFRs in the ferret cortex at P0 [91]. It seems likely that activated FGF receptors in the VZ and the

SVZ resulted in the phenotypes of FGF8-electroporated ferrets. However, it remains possible that other FGFRs are also involved in the pathogenesis of FGF8-electroporated ferrets.

Neural progenitor cells in the cerebral cortex of FGF8-electroporated ferrets

Proliferating cells were increased in the ISVZ and the OSVZ of FGF8-electroporated ferrets (Fig. 12), raising the possibility that the increased proliferating cells are oRGs and/or IPs. To test this possibility, I examined the expression patterns of Pax6, phosphorylated vimentin (pVim) and Tbr2 at P6. Pax6 and pVim are expressed in RGs and oRGs, and Tbr2 is expressed in IPs. I found that Pax6-positive cells were markedly increased in the ISVZ and the OSVZ of FGF8-electroporated ferrets (Fig. 16a, arrows). In addition to an increase in the total number of Pax6-positive cells, their density was also increased in the OSVZ (Fig. 16d). Consistently, pVim-positive cells were increased in the ISVZ and the OSVZ of FGF8-electroporated ferrets (Fig. 16b).

I also examined the percentages of Pax6- and pVim-positive cells. The percentage of Pax6-positive cells was almost double in the cerebral cortex of FGF8-electroporated ferrets (control, 10.1±0.45%; FGF8, 17.7±1.4%; Student's *t*-test, $p<0.01$) (Fig. 17a). Interestingly, the percentage of Pax6-positive cells in FGF8-electroporated ferrets were significantly larger in the OSVZ (control, 10.1±2.9%; FGF8, 22.5±3.1%; Student's *t*-test, $p<0.05$) and in the IZ/CP (control, 0.52±0.029%; FGF8, 12.8±2.2%; Welch's *t*-test, $p<0.05$), whereas that of Pax6-positive cells was not increased in the ISVZ (control, 24.7±2.3%; FGF8, 24.2±4.2%; Student's *t*-test, $p=0.884$) (Fig. 17b-d). The percentage of pVim-positive cells was more than double in the cerebral cortex of FGF8-electroporated ferrets (control, 0.26±0.13%; FGF8,

0.71±0.15%; Student's *t*-test, p<0.05) (Fig. 17e). The percentages of pVim-positive cells in FGF8-electroporated ferrets were not significantly larger in the OSVZ (control, 0.33±0.30%; FGF8, 0.49±0.11%; Student's *t*-test, p=0.5233) and in the ISVZ (control, 0.37±0.072%; FGF8, 0.89±0.38%; Student's *t*-test, p=0.134), whereas were significantly higher in the IZ/CP (control, 0.031±0.022%; FGF8, 0.92±0.26%; Welch's *t*-test, p<0.05) (Fig. 17f-h). I also quantified the percentages of Pax6- and pVim-positive cells in 10 regions along the radial axis from the ventricular surface to the pial surface. The percentages of Pax6-positive cells and pVim-positive cells were significantly increased in upper regions of FGF8-electroporated ferrets. The percentages of Pax6- and pVim-positive cells were significantly larger in region 6,7 and 9 respectively after Bonfferoni correction (Fig. 18b,c), suggesting that oRGs are increased in the cerebral cortex of FGF8-electroporated ferrets, especially in the upper cortical regions. Consistently, Kolmogorov-Smirnov test showed statistically significant difference in the percentages of Pax6-poistive cells between control and FGF8-electroporated ferret (p=0.012).

In the FGF8-electroporated ferret cortex, a number of Ki-67- and pH3-positive cells were found not only in the ISVZ and the OSVZ but also in the IZ and the CP (Fig. 12), where dividing cells are rarely found in the normal ferret cortex. Consistently, I found that Pax6-positive cells and pVim-positive cells appeared in the IZ and CP of FGF8-electroporated ferrets (Fig. 16a,b,e, Fig. 17d,h, Fig. 18b,c), suggesting that oRG-like cells are newly generated in the IZ and CP of FGF8-electroporated ferrets. Currently, although the origin of Pax6- and pVim-positive cells in the IZ and the CP is unknown, it seemed possible that oRGs found in the OSVZ of normal ferrets migrated into the IZ and the CP in FGF8-electroporated ferrets. Future investigations would be

required for uncovering the identities and the roles of oRG-like cells in the IZ and the CP of FGF8-electroporated ferrets.

I also examined the distribution patterns of IPs using anti-Tbr2 antibody (Fig. 16c). Tbr2-positive cells were increased in the SVZ of FGF8-electroporated ferrets (Fig. 16c), suggesting that the number of IPs is also increased in FGF8-electroporated ferrets. I also examined the percentage of Tbr2-positive cells and found that Tbr2 was significantly increased in the IZ/CP (control, 0.094±0.098%; FGF8, 1.1±0.23%; Student's *t*-test, $p<0.01$), whereas that in the OSVZ and that in the ISVZ were not (OSVZ; control, 3.7±1.6%; FGF8, 4.3±0.35%; Student's *t*-test, $p=0.6117$) (ISVZ; control, 8.8±3.7%; FGF8, 6.7±3.0%; Student's *t*-test, $p=0.5781$) (Fig. 17j-l), Consistently, the percentages of Tbr2-positive cells tended to be larger in FGF-electroporated ferrets. Taken together with the results of Pax6 and pVim, my findings indicate that oRGs and IPs are increased in FGF8-electroporated ferrets. It seems likely that these increased oRGs and IPs underlie the pathophysiology of polymicrogyria. On the other hand, I cannot exclude the possibility that displaced RGs are also increased in FGF8-electroporated ferrets. The effects of FGF8 on displaced RGs would be an important issue to be addressed in future research.

Recently, it was reported that there are three kinds of gene expression patterns in progenitors: progenitors expressing Pax6 alone, Tbr2 alone and both Pax6 and Tbr2 [43]. I therefore performed Pax6 and Tbr2 double immunostaining and counted the numbers of each cell type in the IZ and CP. I found that the percentage of Hoechst 33342-positive cells which were Pax6+/Tbr2- was significantly increased in FGF8-electroporated ferrets (control, 1.2±0.3%; FGF8, 17.6±3.9%; Student's *t*-test, $p<0.01$). The percentages of Pax6+/Tbr2+ cells were also increased in

FGF8-electroporated ferrets (control, 0.06±0.06%; FGF8, 1.21±0.43%; Student's *t*-test, $p<0.05$). Pax6-/Tbr2+ cells were comparable between FGF8-electroporated and control ferrets (control, 0%; FGF8, 0.1 ± 0.1%). These results suggest that Pax6-single positive cells and Pax6/Tbr2-double positive cells were increased in FGF8-electroporated ferrets. Consistently, I quantified the number of Pax6+/Tbr2-/pH3+ cells in the OSVZ and found that Pax6+/Tbr2-/pH3+ cells were significantly increased in FGF8-electroporated ferrets (control, 27.5±4.9 cells/mm^2; FGF8, 89.3±19.4 cells/mm^2; Student's *t*-test; $p<0.05$).

It should be noted that although Pax6-positive cells in the cerebral cortex were markedly increased in FGF8-electroporated ferrets, there was a clear decrease in Pax6-positive cells along the ventricular wall (Fig. 16a, Fig. 18b). Consistently, pVim-positive cells tended to be decreased along the ventricular wall in FGF8-electroporated ferrets (Fig. 16b, Fig. 18c). These results suggest that RGs were reduced in the VZ of FGF8-electroporated ferrets. Currently, the reasons for this reduction of RGs in the VZ are unclear, but it is possible that FGF8 induces differentiation of RGs into IPs and oRGs and/or translocation of RGs into the cerebral cortex.

Astrocytes and oligodendrocytes in the cerebral cortex of FGF8-electroporated ferrets

Because astrocytes and oligodendrocytes express FGF receptors [92,93], it seemed possible that astrocytes and oligodendrocytes were affected by the FGF8 signal. I next examined the expression patterns of GFAP and APC, markers for astrocytes and oligodendrocytes, respectively (Fig. 18). Even in the cortical area showing

polymicrogyria, the distribution patterns of GFAP were similar to those in the normal cortex (Fig. 19a). GFAP-positive cells were preferentially located in the cortical surface and the area just under the cortical plates (Fig. 19a). Interestingly, when I quantified the area containing GFAP-positive signals in the cerebral cortex (Fig. 6), I found that the GFAP-positive area was significantly larger in FGF8-electroporated ferrets (control, 5.6±0.78%; FGF8, 15.8±3.4%; Welch's *t*-test; $p < 0.05$) (Fig. 19c). These results suggest that astrocytes were increased in FGF8-electroporated ferrets. It would be intriguing to examine if increased astrocytes are responsible for making additional gyri.

The distribution of oligodendrocytes was revealed with APC staining (Fig. 19b). The distribution patterns of APC were not apparently affected in FGF8-electroporated ferrets. APC was similarly distributed in the white matter in both control and FGF8-electroporated ferrets (Fig. 19b). Olig2 is generally considered to be a marker of the oligodendrocyte lineage, although it was reported that Olig2 is also expressed in putative astrocyte precursors in neonatal rodent brains [94]. Quantification of pH3- and Olig2-double positive cells in Olig2-positive cells did not show significant differences at P6 (Fig. 19d), suggesting that proliferation of Olig2-positive cells is not enhanced in FGF8-electroporated ferrets. These results suggest that oligodendrocytes are not affected in FGF8-electroporated ferrets.

Layer structures of the cerebral cortex of FGF8-electroporated ferrets

To examine the cortical layer structures of polymicrogyria in FGF8-electroporated ferrets, I used anti-NeuN antibody that recognizes post-mitotic neurons. At P36, when polymicrogyria became apparent (Fig. 8), I found two kinds of cortical structures. First, I found polymicrogyria with almost normal cortical layer structures (Fig. 20a).

Interestingly, overall cortical structure revealed with NeuN immunostaining seemed to be preserved. On the other hand, even though the cytoarchitectonic structures of the cerebral cortex seemed normal in FGF8-electroporated ferrets, it remained possible that neuronal identities were affected. I therefore examined the layer markers such as Brn2, Ctip2 and FoxP2. As in the case of mice [95-97], Brn2 was distributed in layers 2/3/5 in the control ferret cortex at P36 (Fig. 20b, control). Ctip2 was predominantly expressed in layer 5 but also in layer 6, whereas FoxP2 was mainly distributed in layer 6 but also in layer 5 (Fig. 20b, control). Consistent with my observation using NeuN staining, Brn2 immunostaining showed normal 6-layered structures in the cortical area with polymicrogyria in FGF8-electroporated ferrets (Fig. 20b). Ctip2 and FoxP2 immunostaining also showed that the cortical area with polymicrogyria in FGF8-electroporated ferrets contained apparently normal layers 5 and 6 (Fig. 20b, arrowheads). These results suggest that neuronal identities are not affected in FGF8-electroporated ferrets. Although the cortical layer structures of polymicrogyria in FGF8-electroporated ferrets were preserved, it seemed possible that the thicknesses of cortical layers were affected differently in FGF8-electroporated ferrets. To test this possibility, I measured the average thicknesses of layers 2/3, 4 and 5/6 in coronal sections at P36. Interestingly, I found that layer 2/3 was significantly thicker in FGF8-electroporated ferrets (control, 582 ± 23 μm; FGF8, 708 ± 52 μm; Student's *t*-test; $p < 0.05$) (Fig. 20e). In contrast, the thicknesses of layer 4 and layer 5/6 were not increased in FGF8-electroporated ferrets (Fig. 20f,g). These results suggest that layer 2/3 was preferentially increased compared with other layers in FGF8-electroporated ferrets. The increase in layer 2/3 could be involved in the formation of polymicrogyria in FGF8-electroporated ferrets.

Second, I also found polymicrogyria in which layer 2/3 was predominantly distorted, but in which other layers seemed less affected (Fig. 20c, arrows). Overproduction of layer 2/3 neurons could result from enhanced cell proliferation at the later stage of cortical development. Beside polymicrogyria, it has been reported that human TD patients also have subependymal heterotopia [22], which is the presence of heterotopic nodules situated close to the lateral ventricle. Consistently, I found heterotopic nodules close to the lateral ventricle in the cerebral cortex of FGF8-electroporated ferrets (Fig. 20d, arrows). Interestingly, the subependymal heterotopia in FGF8-electroporated ferrets was NeuN-positive, suggesting that subependymal heterotopia contains many post-mitotic neurons.

Discussion

I have shown that all of FGF8-transfected ferrets have polymicrogyria, megalencephaly and subependymal heterotopia to a greater or lesser extent, which are common features of human TD patients. My histological analyses indicate that oRGs and IPs are increased in the SVZ of FGF8-electroporated ferrets. Polymicrogyria seemed to result from increased numbers of oRGs and IPs. My findings also suggest that FGF8-electroporated ferrets have increased astrocytes and thickening in layer 2/3, which could be involved in the pathogenesis of polymicrogyria.

Pathophysiology of the cortical malformation of TD

Because embryonic and neonatal samples of human TD patients are often difficult to be obtained, the mechanisms underlying of the cortical malformation of TD patients are still largely unclear. Because embryonic and neonatal ferret samples are available, FGF8-electroporated ferrets enabled me to investigate the pathophysiological mechanisms of TD patients. Polymicrogyria of FGF8-electroporated ferrets has normal layer structures except for the increased thickness of layer 2/3. Interestingly, previous studies reported polymicrogyria containing the unlayered cortex and that containing the 4-layered cortex depending on their causes. These different histological features raises the possibility that polymicrogyria can be elicited by multiple cellular mechanisms. It would be intriguing to uncover the entire mechanisms underlying polymicrogyria. I also found periventricular nodular heterotopia (PNH) in the cerebral cortex of FGF8-electroporated ferrets. As in the case of PNH in human patients with FGFR3 overactivation, PNH in FGF8-electroporated ferrets was NeuN-positive [20].

I found that cell proliferation was significantly enhanced, and oRGs and IPs were increased in neonatal FGF8-electroporated ferrets. A recent work reported that progenitor cells were increased in the cortex in human TD patients, but detailed information about the identities of progenitor cells were unclear [98]. A previous pioneering work clearly demonstrated that IPs were increased in TD-CNS mice [36]. In addition to IPs, I uncovered that oRGs are increased in FGF8-electroporated ferrets. Therefore, it would be intriguing to examine the expression of Pax6 and pVim in human TD patients. In addition, I found oRG-like cells in the IZ and the CP of FGF8-electroporated ferrets. The origin and the role of these cells in the pathophysiology of TD patients would be interesting to examine.

My findings showed that the number of astrocytes and the thickness of layer 2/3 were preferentially increased in FGF8-electroporated ferrets. It seems likely that increased oRGs and IPs result in the overproduction of layer 2/3 neurons and astrocytes. Previously, it has been hypothesized that the appearance of cortical gyri was produced by an increase in superficial layers relative to deep layers of the cerebral cortex [58,85]. My finding is consistent with this hypothesis. In addition, my findings raise the possibility that the increase in astrocytes is involved in the formation of cortical gyri. Although the amount of astrocytes compared to that of neurons in the cortex gradually increased with evolution [99], little attention has been paid to the role of astrocytes in the production of cortical gyri. It would be extremely important to examine the roles of oRGs, IPs, upper cortical neurons and astrocytes in the formation of cortical gyri.

There have been two hypotheses about the pathophysiology of TD patients [22]. It has been suggested that activated FGF signaling in the brain leads to the brain phenotype of TD patients. Alternatively, it was also proposed that the brain phenotype

of TD patients is a secondary deformation caused by skull defects such as craniosynostosis. A previous report using mice showed that genetic manipulations that introduce a TD mutation only in the nervous system led to megalencephaly, suggesting that megalencephaly results from activated FGF signaling in the brain [35]. In contrast to megalencephaly, because polymicrogyria was not obvious in TD-CNS mice [34,35], it was difficult to address which hypotheses accounted for the pathophysiology of polymicrogyria using TD-CNS mice. Because I expressed FGF8 only in the nervous system, my study using FGF8-electroporated ferrets directly indicate that as in the case of megalencephaly, FGF signaling in the brain is responsible for polymicrogyria. Consistently, the gyral abnormalities in human TD patients become evident before synostosis occurs during development.

Activation of FGF signaling produces polymicrogyria in ferrets

I found that activation of FGF signaling results in polymicrogyria in ferrets. Because I also found that oRGs and IPs were increased in the developing cortex of FGF8-electroporated ferrets, one attractive hypothesis would be that increased oRGs are responsible for polymicrogyria of FGF8-electroporated ferrets. Consistently, it has been proposed that increased number of oRGs led to the emergence of gyrencephalic cortex during evolution [84,85,88,89]. Because it has been demonstrated that activation of FGF signaling increases cell proliferation of progenitor cells in the developing cortex [37,65,100-102], it seems plausible that activation of FGF signaling leads to the proliferation of oRGs. In addition, it seems possible that differentiation from neural progenitors to post-mitotic neurons is affected by FGF activation, and this could also mediate the increase in neural progenitors.

Instead of FGF8, the constitutively active form of FGFR3 (caFGFR3) was an alternative choice to be expressed. However, I did not choose caFGFR3 mainly because of the following two reasons. The first reason is that introduction of caFGFR3 by *in utero* electroporation activate FGF signaling even in cells which do not express endogenous FGFR3. In contrast, introduction of FGF8 activate FGF signaling only in cells expressing endogenous FGFR because FGF8 can work only by activating endogenous FGFR. The second reason is that transfected caFGFR3 works cell-autonomously, whereas FGF8 works on not only transfected cells but also on neighboring cells because FGF8 is supposed to be secreted from transfected cells. FGF8 therefore activates FGF signaling in a larger number of cells than caFGFR3, and as a result, I thought that macroscopic morphological changes of cortical folding could be more obvious using FGF8 rather than caFGFR3.

Advantages of ferrets for examining the mechanisms of TD

Previously, it was reported that TD-CNS mice showed megalencephaly, but failed to exhibit polymicrogyria [34,35]. In contrast, my FGF8-electroporated ferrets have obvious polymicrogyria. Currently, the reasons for this discrepancy between ferrets and mice are unclear, but it seems plausible that mice do not have the mechanisms responsible for making polymicrogyria because the cortical gyrus is missing in normal mice. Ferrets seem to be more appropriate for investigating the pathophysiology of cortical malformations.

Ferrets have several advantages. First, the brain of ferrets has been widely used for anatomical and electrophysiological experiments, so anatomical and electrophysiological data are available. The anatomical structures of cortical gyri and

sulci are well described [83]. Second, the developmental processes of cortical gyri have been revealed [83]. Notably, when ferret babies are born, their brains are lissencephalic, and cortical gyri and sulci are formed after birth. Therefore, the mechanisms of the formation and malformation of cortical gyri can be examined using neonatal ferrets rather than embryos. Third, usually 6-10 babies are born from one ferret pregnant mother. This large number of babies per ferret pregnant mother provides opportunities to test various experimental conditions.

In addition to polymicrogyria, ferrets might be also useful for investigating the pathophysiology of cortical malformations such as lissencephaly and pachygyria and neurological disorders like schizophrenia and autism. It would be intriguing to investigate behavioral phenotypes in ferret models of cortical malformation. As exemplified in this study, genetic manipulations of ferrets using *in utero* electroporation should be useful for neuroscience experiments using gyrencephalic higher mammals.

Acknowledgments

I am grateful to Dr. H. Kawasaki (Kanazawa University), Drs. S. Tsuji, T. Kadowaki, H. Bito (The University of Tokyo) for their continuous support and warm encouragement. I express my gratitude to Drs. Y. Shinmyo, T. Sakurai and M. Sato (Kanazawa University) and Dr. T. Saito (Chiba University) for their technical support. I thank Kawasaki lab members for critical discussions and comments.

Note

The contents of this thesis were published in Scientific Reports.

References

1. Poduri A, Evrony GD, Cai X, and Walsh CA. Somatic mutation, genomic variation, and neurological disease. Science 341, 1237758 (2013).

2. Barkovich AJ, Kuzniecky RI, Jackson GD, Guerrini R, and Dobyns WB. A developmental and genetic classification for malformations of cortical development. Neurology 65, 1873–1887 (2005).

3. Barkovich AJ, Guerrini R, Kuzniecky RI, Jackson GD, and Dobyns WB. A developmental and genetic classification for malformations of cortical development: update 2012. Brain 135, 1348–1369 (2012).

4. Barkovich AJ. Current concepts of polymicrogyria. Neuroradiology 52, 479–487 (2010).

5. Guerrini R, and Marini C. Genetic malformations of cortical development. Exp. Brain Res. 173, 322–333 (2006).

6. Mochida GH and Walsh CA. Genetic basis of developmental malformations of the cerebral cortex. Arch. Neurol. 61, 637–640 (2004).

7. Francis F, Meyer G, Fallet-Bianco C, Moreno S, Kappeler C, Socorro AC, Tuy FP, Beldjord C, and Chelly J. Human disorders of cortical development: from past to

present. Eur. J. Neurosci. 23, 877–893 (2006).

8. Barkovich AJ, Gressens P, and Evrard P. Formation, maturation, and disorders of brain neocortex. Am. J. Neuroradiol. 13, 423– 446 (1992).

9. Golden JA, Harding BN. Cortical malformations: unfolding polymicrogyria. Nat. Rev. Neurol. 6, 471-472 (2010).

10. Barkovich AJ, Millen KJ, and Dobyns WB. A developmental classification of malformations of the brainstem. Ann. Neurol. 62, 625–639 (2007).

11. Wieck G, Leventer RJ, Squier WM, Jansen A, Andermann E, Dubeau F, Ramazzotti A, Guerrini R, and Dobyns WB. Periventricular nodular heterotopia with overlying polymicrogyria. Brain 128, 2811–2821 (2005).

12. Barkovich AJ. Morphology of subcortical heterotopia: a magnetic resonance study. Am. J. Neuroradiol. 21, 290–295 (2000).

13. Dobyns WB, Mirzaa G, Christian SL, Petras K, Roseberry J, Clark GD, Curry CJ, McDonald-McGinn D, Medne L, Zackai E, Parsons J, Zand DJ, Hisama FM, Walsh CA, Leventer RJ, Martin CL, Gajecka M, and Shaffer LG. Consistent chromosome abnormalities identify novel polymicrogyria loci in 1p36.3, 2p16.1–p23.1, 4q21.21–q22.1, 6q26–q27, and 21q2. Am. J. Med. Genet. Part A 146A, 1637–1654

(2008).

14. Guerrini R, Dravet C, Raybaud C, Roger J, Bureau M, Battaglia A, Livet MO, Gambarelli D, and Robain O. Epilepsy and focal gyral anomalies detected by MRI: electroclinico-morphological correlations and follow-up. Dev. Med. Child Neurol. 34, 706–718 (1992).

15. Barkovich AJ, and Kjos BO. Non-lissencephalic cortical dysplasia: correlation of imaging findings with clinical deficits. Am. J. Neuroradiol. 13, 95–103 (1992).

16. Guerrini R, Dubeau F, Dulac O, Barkovich AJ, Kuzniecky R, Fett C, Jones-Gotman M, Canapicchi R, Cross H, Fish D, Bonanni P, Jambaqué I, and Andermann F. Bilateral parasagittal parietooccipital polymicrogyria and epilepsy. Ann. Neurol. 41, 65–73 (1997).

17. Hayashi N, Tsutsumi Y, and Barkovich AJ. Morphological features and associated anomalies of schizencephaly in the clinical population: detailed analysis of MR images. Neuroradiology 44, 418–427 (2002).

18. Guerrini R, and Filippi T. Neuronal migration disorders, genetics, and epileptogenesis. J. Child Neurol. 20, 287–299 (2005).

19. Parrini E, Ramazzotti A, Dobyns WB, Mei D, Moro F, Veggiotti P, Marini C,

Brilstra EH, Dalla Bernardina B, Goodwin L, Bodell A, Jones MC, Nangeroni M, Palmeri S, Said E, Sander JW, Striano P, Takahashi Y, Van Maldergem L, Leonardi G, Wright M, Walsh CA, and Guerrini R. Periventricular heterotopia: phenotypic heterogeneity and correlation with Filamin A mutations. Brain 129, 1892-1906 (2006).

20. Hevner RF. Brain overgrowth in disorders of RTK-PI3K-AKT signaling: A mosaic of malformations. Semin. Perinatol. 30, 36-43 (2015).

21. Broix L, Jagline H, L vanova E, Schmucker S, Drouot N, Clayton-Smith J, Pagnamenta AT, Metcalfe KA, Isidor B, Louvier UW, Poduri A, Taylor JC, Tilly P, Poirier K, Saillour Y, Lebrun N, Stemmelen T, Rudolf G, Muraca G, Saintpierre B, Elmorjani A. Mutations in the HECT domain of NEDD4L lead to AKT-mTOR pathway deregulation and cause periventricular nodular heterotopia. Nat. Genet. 48, 1349-1358 (2016).

22. Hevner RF. The cerebral cortex malformation in thanatophoric dysplasia: neuropathology and pathogenesis. Acta Neuropathol. 110, 208–221 (2005).

23. Vogt C, and Blaas HG. Thanatophoric dysplasia: autopsy findings over a 25-year period. Pediatr. Dev. Pathol. 16, 160–167 (2013).

24. Tavormina PL, Shiang R, Thompson LM, Zhu YZ, Wilkin DJ, Lachman RS, Wilcox WR, Rimoin DL, Cohn DH, and Wasmuth JJ. Thanatophoric dysplasia (types I and II) caused by distinct mutations in fibroblast growth factor receptor 3. Nat. Genet. 9, 321–328 (1995).

25. Rousseau F, Saugier P, Le Merrer M, Munnich A, Delezoide AL, Maroteaux P, Bonaventure J, Narcy F, and Sanak M. Stop codon FGFR3 mutations in thanatophoric dwarfism type 1. Nat. Genet. 10, 11–12 (1995).

26. Shiang R, Thompson LM, Zhu YZ, Church DM, Fielder TJ, Bocian M, Winokur ST, and Wasmuth JJ. Mutations in the transmembrane domain of FGFR3 cause the most common genetic form of dwarfism, achondroplasia. Cell 78, 335–342 (1994).

27. Bellus GA, McIntosh I, Smith EA, Aylsworth AS, Kaitila I, Horton WA, Greenhaw GA, Hecht JT, and Francomano CA.. A recurrent mutation in the tyrosine kinase domain of fibroblast growth factor receptor 3 causes hypochondroplasia. Nat. Genet. 10, 357–359 (1995).

28. Rousseau F, Bonaventure J, Legeai-Mallet L, Pelet A, Rozet JM, Maroteaux P, Le Merrer M, and Munnich A. Mutations in the gene encoding fibroblast growth factor receptor-3 in achondroplasia. Nature 371, 252–254 (1994).

29. Francomano CA, Ortiz de Luna RI, Hefferon TW, Bellus GA, Turner CE, Taylor E, Meyers DA, Blanton SH, Murray JC, McIntosh I, and Hecht JT. Localization of the achondroplasia gene to the distal 2.5 Mb of human chromosome 4p. Hum. Mol. Genet. 3, 787–792 (1994).

30. Lachman RS. International nomenclature and classification of the osteochondrodysplasias (1997). Pediatr. Radiol. 28, 737– 744 (1998).

31. Hall CM. International nosology and classification of constitutional disorders of bone. Am. J. Med. Genet. 113, 65–77 (2002).

32. Webster MK, D'Avis PY, Robertson SC and Donoghue DJ. Profound ligand-independent kinase activation of fibroblast growth factor receptor 3 by the activation loop mutation responsible for a lethal skeletal dysplasia, thanatophoric dysplasia type II. Mol. Cell. Biol. 16, 4081–4087 (1996).

33. Naski MC, Wang Q, Xu J, and Ornitz DM. Graded activation of fibroblast growth factor receptor 3 by mutations causing achondroplasia and thanatophoric dysplasia. Nat. Genet. 13, 233–237 (1996).

34. Inglis-Broadgate SL, Thomson RE, Pellicano F, Tartaglia MA, Pontikis CC, Cooper JD, and Iwata T. FGFR3 regulates brain size by controlling progenitor cell

proliferation and apoptosis during embryonic development. Dev. Biol. 279, 73–85 (2005).

35. Lin T, Sandusky SB, Xue H, Fishbein KW, Spencer RG, Rao MS, and Francomano CA. A central nervous system specific mouse model for thanatophoric dysplasia type II. Hum. Mol. Genet. 12, 2863–2871 (2003).

36. Thomson RE, Kind PC, Graham NA, Etherson ML, Kennedy J, Fernandes AC, Marques CS, Hevner RF, and Iwata T. Fgf receptor 3 activation promotes selective growth and expansion of occipitotemporal cortex. Neural Dev. 4, 4 (2009).

37. Iwata T, and Hevner RF. Fibroblast growth factor signaling in development of the cerebral cortex. Dev. Growth Differ. 51, 299–323 (2009).

38. Iwata T, Chen L, Li C, Ovchinnikov DA, Behringer RR, Francomano CA and Deng CX. A neonatal lethal mutation in FGFR3 uncouples proliferation and differentiation of growth plate chondrocytes in embryos. Hum. Mol. Genet. 9, 1603–1613 (2000).

39. Kawasaki H, Crowley JC, Livesey FJ, and Katz LC. Molecular organization of the ferret visual thalamus. J. Neurosci. 24, 9962–9970 (2004).

40. Iwai L, and Kawasaki H. Molecular development of the lateral geniculate nucleus in

the absence of retinal waves during the time of retinal axon eye-specific segregation. Neuroscience 159, 1326–1337 (2009).

41. Iwai L, Ohashi Y, van der List D, Usrey WM, Miyashita Y, and Kawasaki H. FoxP2 is a parvocellular-specific transcription factor in the visual thalamus of monkeys and ferrets. Cereb. Cortex 23, 2204–2212 (2013).

42. Fujishiro T, Kawasaki H, Aihara M, Saeki T, Ymagishi R, Atarashi T, Mayama C, and Araie M. Establishment of an experimental ferret ocular hypertension model for the analysis of central visual pathway damage. Sci. Rep. 4, 6501 (2014).

43. Kawasaki H, Toda T, and Tanno K. In vivo genetic manipulation of cortical progenitors in gyrencephalic carnivores using in utero electroporation. Biol. Open 2, 95–100 (2013).

44. Kawasaki H, Iwai L, and Tanno K. Rapid and efficient genetic manipulation of gyrencephalic carnivores using in utero electroporation. Mol. Brain 5, 24 (2012).

45. Hartfuss E, Galli R, Heins N, and Götz M. Characterization of CNS precursor subtypes and radial glia. Dev. Biol. 229, 15–30 (2001).

46. Noctor SC, Flint AC, Weissman TA, Wong WS, Clinton BK, and Kriegstein AR. Dividing precursor cells of the embryonic cortical ventricular zone have

morphological and molecular characteristics of radial glia. J. Neurosci. 22, 3161–3173 (2002).

47. Noctor SC, Martínez-Cerdeño V, Ivic L, and Kriegstein AR. Cortical neurons arise in symmetric and asymmetric division zones and migrate through specific phases. Nat. Neurosci. 7, 136–144 (2004).

48. Haubensak W, Attardo A, Denk W, and Huttner WB. Neurons arise in the basal neuroepithelium of the early mammalian telencephalon: a major site of neurogenesis. Proc. Natl. Acad. Sci. USA 101, 3196–3201 (2004).

49. Kowalczyk T, Pontious A, Englund C, Daza RA, Bedogni F, Hodge R, Attardo A, Bell C, Huttner WB, and Hevner RF. Intermediate neuronal progenitors (basal progenitors) produce pyramidal-projection neurons for all layers of cerebral cortex. Cereb. Cortex 19, 2439–2450 (2009).

50. Fish JL, Dehay C, Kennedy H, and Huttner WB. Making bigger brains - the evolution of neural-progenitor-cell division. J. Cell Sci. 121, 2783– 2793 (2008).

51. Smart IH, Dehay C, Giroud P, Berland M, and Kennedy H. Unique morphological features of the proliferative zones and postmitotic compartments of the neural epithelium giving rise to striate and extrastriate cortex in the monkey. Cereb.

Cortex 12, 37–53 (2002).

52. Zecevic N, Chen Y, and Filipovic R. Contributions of cortical subventricular zone to the development of the human cerebral cortex. J. Comp. Neurol. 491, 109–122 (2005).

53. Englund C, Fink A, Lau C, Pham D, Daza RA, Bulfone A, Kowalczyk T, and Hevner RF. Pax6, Tbr2, and Tbr1 are expressed sequentially by radial glia, intermediate progenitor cells, and postmitotic neurons in developing neocortex. J. Neurosci. 25, 247–251 (2005).

54. Hansen DV, Lui JH, Parker PR, and Kriegstein AR. Neurogenic radial glia in the outer subventricular zone of human neocortex. Nature 464, 554–561 (2010).

55. Fietz SA, Kelava I, Vogt J, Wilsch-Bräuninger M, Stenzel D, Fish JL, Corbeil D, Riehn A, Distler W, Nitsch R, and Huttner WB. OSVZ progenitors of human and ferret neocortex are epithelial-like and expand by integrin signaling. Nat. Neurosci. 13, 690–699 (2010).

56. Kriegstein A, Noctor S, and Martínez-Cerdeño V. Patterns of neural stem and progenitor cell division may underlie evolutionary cortical expansion. Nat. Rev. Neurosci. 7, 883–890 (2006).

57. Reillo I, de Juan Romero C, Garcia-Cabezas MA, and Borrell V. A role for intermediate radial glia in the tangential expansion of the mammalian cerebral cortex. Cereb. Cortex 21, 1674–1694 (2010).

58. Muramatsu T, Mizutani Y, Ohmori Y and Okumura J. Comparison of three nonviral transfection methods for foreign gene expression in early chicken embryos *in ovo*. Biochem. Biophys. Res. Commun. 230, 376–380 (1997).

59. Itasaki N, Bel-Vialar S and Krumlauf R. "Shocking" developments in chick embryology: Electroporation and *in ovo* gene expression. Nat. Cell Biol. 1, 203–207 (1999).

60. Swatrtz M, Eberhart J, Mastick GS and Krull CE. Sparking new frontiers: Using in vivo electroporation for genetic manipulation. Dev. Biol. 233, 13–21 (2001).

61. Saito T, Nakatsuji N. Efficient gene transfer into the embryonic mouse brain using in vivo electroporation. Dev. Biol. 240, 237-46 (2001).

62. Tabata H, Nakajima K. Efficient in utero gene transfer system to the developing mouse brain using electroporation: visualization of neuronal migration in the developing cortex. Neuroscience. 103, 865-872 (2001).

63. Fukuchi-Shimogori T, Grove EA. Neocortex patterning by the secreted signaling molecule FGF8. Science. 294, 1071-1074 (2001).

64. Ford-Perriss M, Abud H, and Murphy M. Fibroblast growth factors in the developing central nervous system. Clin. Exp. Pharmacol. Physiol. 28, 493–503 (2001).

65. Guillemot F, Zimmer C. From cradle to grave: the multiple roles of fibroblast growth factors in neural development. Neuron. 71, 574-588 (2011).

66. Vaccarino FM, Schwartz ML, Raballo R, Nilsen J, Rhee J, Zhou M, Doetschman T, Coffin JD, Wyland JJ, Hung YT. Changes in cerebral cortex size are governed by fibroblast growth factor during embryogenesis. Nat. Neurosci. 2, 246–253 (1999).

67. Mansour SL, Goddard JM, Capecchi MR. Mice homozygous for a targeted disruption of the proto-oncogene int-2 have developmental defects in the tail and inner ear. Development. 117, 13–28 (1993).

68. McKay IJ, Lewis J, Lumsden A. The role of FGF-3 in early inner ear development: An analysis in normal and kreisler mutant mice. Dev. Biol. 174, 370–378 (1996).

69. Wang JK, Gao G, Goldfarb M. Fibroblast growth factor receptors have different signaling and mitogenic potentials. Mol. Cell. Biol. 14, 181-188 (1994).

70. Vainikka S, Joukov V, Wenstom S, Bergman M, Pelicci PG, Alitalo K. Signal transduction by fibroblast growth factor receptor-4 (FGFR-4). Comparison with FGFR-1. J. Biol. Chem. 269, 18320-18326 (1994).

71. Seuntjens E, Nityanandam A, Miquelajauregui A, Debruyn J, Stryjewska A, Goebbels S, Nave KA, Huylebroeck D and Tarabykin V. Sip1 regulates sequential fate decisions by feedback signaling from postmitotic neurons to progenitors. Nat. Neurosci. 12, 1373–1380 (2009).

72. Reuss B, von Bohlen und Halbach O. Fibroblast growth factors and their receptors in the central nervous system. Cell. Tissue Res. 313 139-157 (2003).

73. Olsen SK, Li JYH, Bromleigh C, Eliseenkova AV, Ibrahimi OA, Lao Z, Zhang F, Linhardt RJ, Joyner AL and Mohammadi M. Structural basis by which alternative splicing modulates the organizer activity of FGF8 in the brain. Genes. Dev. 20, 185-198 (2006).

74. Ghosh AK, Shankar DB, Shackleford GM, Wu K, T'Ang A, Miller GJ, Zheng J, Roy-Burman P. Molecular cloning and characterization of human FGF8 alternative messenger RNA forms. Cell Growth. Differ. 7, 1425-1434 (1996).

75. Reillo I, and Borrell V. Germinal zones in the developing cerebral cortex of ferret: ontogeny, cell cycle kinetics, and diversity of progenitors. Cereb. Cortex 22, 2039–2054 (2012).

76. Sehara K, Toda T, Iwai L, Wakimoto M, Tanno K, Matsubayashi Y, and Kawasaki H. Whisker-related axonal patterns and plasticity of layer 2/3 neurons in the mouse barrel cortex. J. Neurosci. 30, 3082–3092 (2010).

77. Kawasaki H, Mizuseki K, Nishikawa S, Kaneko S, Kuwana Y, Nakanishi S, Nishikawa SI, and Sasai Y. Induction of midbrain dopaminergic neurons from ES cells by stromal cell-derived inducing activity. Neuron 28, 31–40 (2000).

78. Toda T, Homma D, Tokuoka H, Hayakawa I, Sugimoto Y, Ichinose H, and Kawasaki H. Birth regulates the initiation of sensory map formation through serotonin signaling. Dev. Cell 27, 32–46 (2013).

79. Wakimoto M, Sehara K, Ebisu H, Hoshiba Y, Tsunoda S, Ichikawa Y, and Kawasaki H. Classic cadherins mediate selective intracortical circuit formation in the mouse neocortex. Cereb. Cortex. 25, 3535-3546 (2015).

80. Zilles K, Armstrong E, Moser KH, Schleicher A and Stephan H. Gyrification in the cerebral cortex of primates. Brain Behav. Evol. 34, 143–150 (1989).

81. Zhang X, Ibrahimi OA, Olsen SK, Umemori H, Mohammadi M, Ornitz DM. Receptor specificity of the fibroblast growth factor family. The complete mammalian FGF family. J. Biol. Chem. 281, 15694–15700 (2006).

82. Ornitz DM, Xu J, Colvin JS, McEwen DG, MacArthur CA, Coulier F, Gao G, Goldfarb M. Receptor specificity of the fibroblast growth factor family. J. Biol. Chem. 271, 15292–15297 (1996).

83. Smart IH, and McSherry GM. Gyrus formation in the cerebral cortex in the ferret. I. Description of the external changes. J. Anat. 146, 141–152 (1986).

84. Hevner RF, and Haydar TF. The (not necessarily) convoluted role of basal radial glia in cortical neurogenesis. Cereb. Cortex 22, 465–468 (2012).

85. Lui JH, Hansen DV, and Kriegstein AR. Development and evolution of the human neocortex. Cell 146, 18–36 (2011).

86. Molnar Z, and Clowry G. Cerebral cortical development in rodents and primates. Prog. Brain Res. 195, 45–70 (2012).

87. Dehay C, and Kennedy H. Cell-cycle control and cortical development. Nat. Rev. Neurosci. 8, 438–450 (2007).

88. Fietz SA, and Huttner WB. Cortical progenitor expansion, self-renewal and neurogenesis-a polarized perspective. Curr. Opin. Neurobiol. 21, 23–35 (2011).

89. Borrell V, and Reillo I. Emerging roles of neural stem cells in cerebral cortex development and evolution. Dev. Neurobiol. 72, 955–971 (2012).

90. Rakic P. Evolution of the neocortex: a perspective from developmental biology. Nat. Rev. Neurosci. 10, 724–735 (2009).

91. de Juan Romero C, Bruder C, Tomasello U, Sanz-Anquela JM, and Borrell V. Discrete domains of gene expression in germinal layers distinguish the development of gyrencephaly. EMBO. J. 34, 1859–1874 (2015).

92. Miyake A, Konishi M, Martin FH, Hernday NA, Ozaki K, Yamamoto S, Mikami T, Arakawa T, Itoh N. Structure and expression of a novel member, FGF-16, on the fibroblast growth factor family. Biochem. Biophys. Res. Commun. 4, 148-152 (1998).

93. Reuss B, Unsicker K. Survival and differentiation of dopaminergic mesencephalic neurons are promoted by dopamine-mediated induction of FGF-2 in striatal astroglial cells. Mol. Cell. Neurosci. 16, 781-792 (2000).

94. Marshall CA, Novitch BG, and Goldman JE. Olig2 directs astrocyte and oligodendrocyte formation in postnatal subventricular zone cells. J. Neurosci. 25, 7289–7298 (2005).

95. Hevner RF, Daza RA, Rubenstein JL, Stunnenberg H, Olavarria JF, and Englund C. Beyond laminar fate: toward a molecular classification of cortical projection/pyramidal neurons. Dev. Neurosci. 25, 139–151 (2003).

96. Arlotta P, Molyneaux BJ, Chen J, Inoue J, Kominami R, and Macklis JD. Neuronal subtype-specific genes that control corticospinal motor neuron development in vivo. Neuron 45, 207–221 (2005).

97. Ferland RJ, Cherry TJ, Preware PO, Morrisey EE, and Walsh CA. Characterization

of Foxp2 and Foxp1 mRNA and protein in the developing and mature brain. J. Comp. Neurol. 460, 266–279 (2003).

98. Itoh K, Pooh R, Kanemura Y, Yamasaki M, and Fushiki S. Brain malformation with loss of normal FGFR3 expression in thanatophoric dysplasia type I. Neuropathology 33, 663–666 (2013).

99. Nedergaard M, Ransom B, and Goldman SA. New roles for astrocytes: redefining the functional architecture of the brain. Trends Neurosci. 26, 523–530 (2003).

100. Gotz M, and Huttner WB. The cell biology of neurogenesis. Nat. Rev. Mol. Cell Biol. 6, 777–788 (2005).

101. Rubenstein JL. Annual Research Review: Development of the cerebral cortex: implications for neurodevelopmental disorders. J. Child Psychol. Psychiatry 52, 339–355 (2011).

102. Vaccarino FM, Grigorenko EL, Smith KM, and Stevens HE. Regulation of cerebral cortical size and neuron number by fibroblast growth factors: implications for autism. J. Autism Dev. Disord. 39, 511–520 (2009).

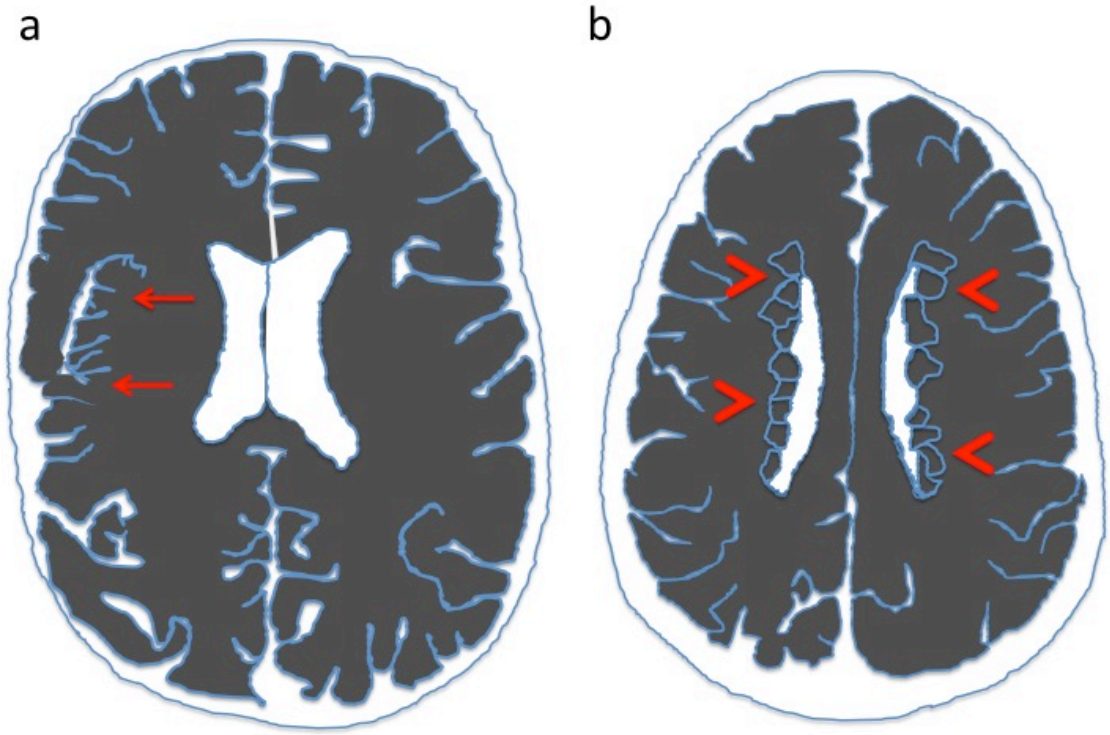

Figure 1. Polymicrogyria and periventricular nodular heterotopia.

(**a**) A scheme of polymicrogyria (arrows). (**b**) A scheme of periventricular nodular heterotopia. Heterotopic nodules are located along the ventricular walls (arrowheads).

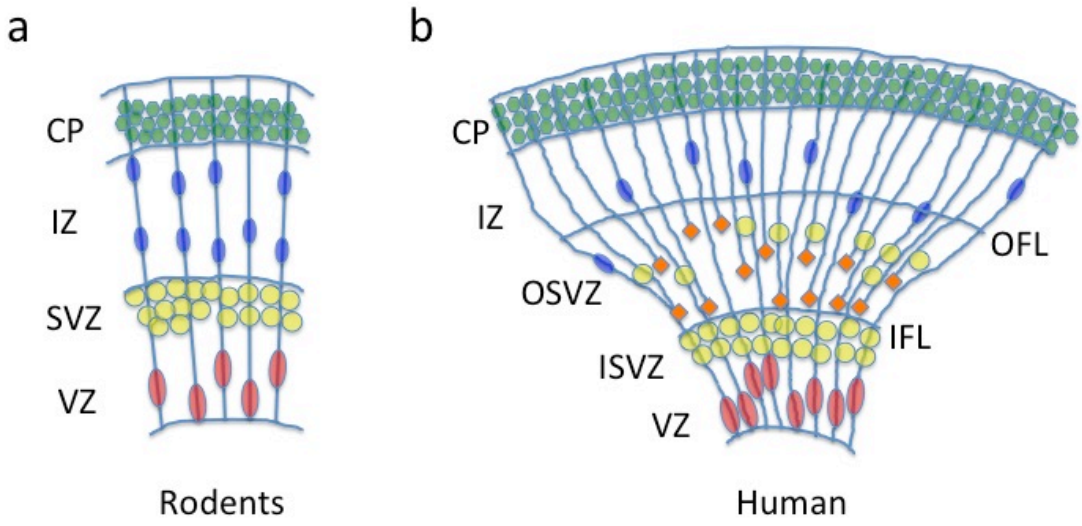

Figure 2. The developing neocortex of rodents and primates.

(**a**) A scheme of rodent corticogenesis is illustrated. Radial glial cells (RGs, red) produce intermediate progenitor cells (IPs, yellow), that generate two neurons (blue). These neurons migrate to the cortical plate using RG fibers. (**b**) A scheme of human corticogenesis is illustrated. The scheme shows oRGs (orange), IPs (yellow), migrating neurons (blue), mature neuron (green) and increased RG fibers. CP, cortical plate; IZ, intermediate zone; SVZ, subventricular zone; OSVZ, outer subventricular zone; ISVZ, inner subventricular zone; VZ, ventricular zone; OFL, outer fiber layer; IFL, inner fiber layer.

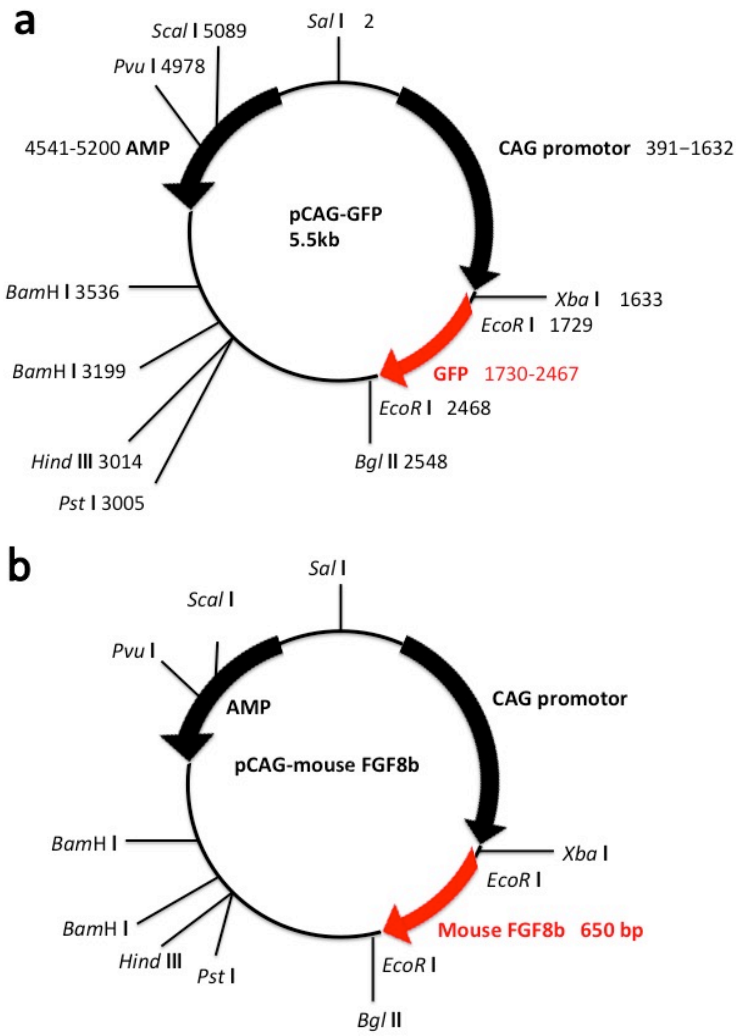

Fig 3. The structures of plasmids. (a) pCAG-GFP. The CAG promotor drives the expression of GFP. (b) pCAG-FGF8b. To make pCAG-FGF8b, the GFP sequence on pCAG-GFP were replaced with mouse FGF8b sequence by using *EcoRI*.

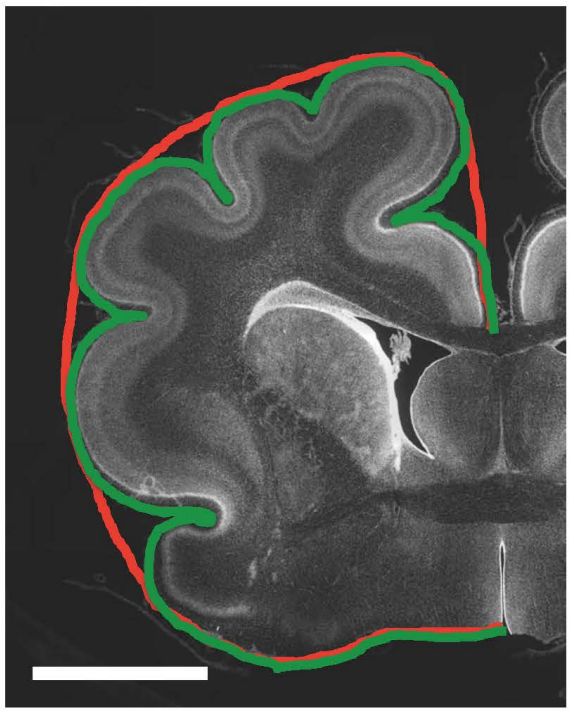

Figure 4. The definition of the GI value.

After *in utero* electroporation was performed, brains were prepared at P16 and P36. Coronal sections containing the anterior part of the lateral ventricle were stained with Hoechst 33342 (white). The GI value was the length of the complete contour (green line) divided by that of the outer contour (red line). Scale bar = 6 mm.

Figure 5. The definition of the GN value. After *in utero* electroporation was performed, brains were prepared at P16 and P36. Coronal sections containing the anterior part of the lateral ventricle were stained with Hoechst 33342 (white). The GN value indicates how many times the complete contour (green line) was detached from the outer contour (red line) of the brain (i.e. the number of asterisks). The GN value = the number of asterisks. The GNt value = the GN of transfected side. The GNo value = the GN of the other side. Scale bar = 6 mm.

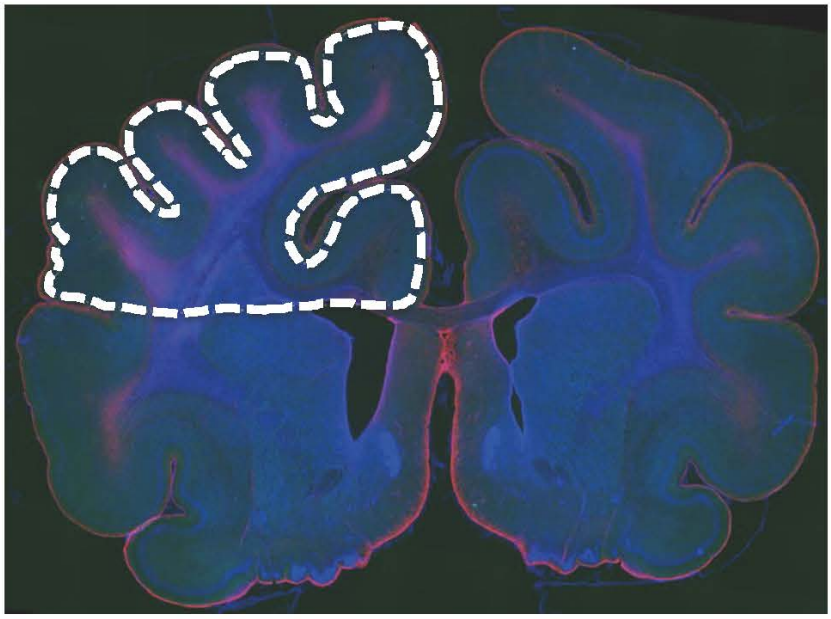

Figure 6. Quantification of the GFAP-positive area in the cerebral cortex. After *in utero* electroporation was performed, brains were prepared at P36. Coronal sections containing the anterior part of the lateral ventricle were stained with anti-GFAP antibody (red) and Hoechst 33342 (blue). The region of the cortical hemisphere located dorsal to the corpus callosum was selected, and the selection excluded the cortical surface. The total area (area within the broken line) and the GFAP-positive area (red area within the broken line) were measured. Then, the value of the GFAP-positive area was divided by that of the total area.

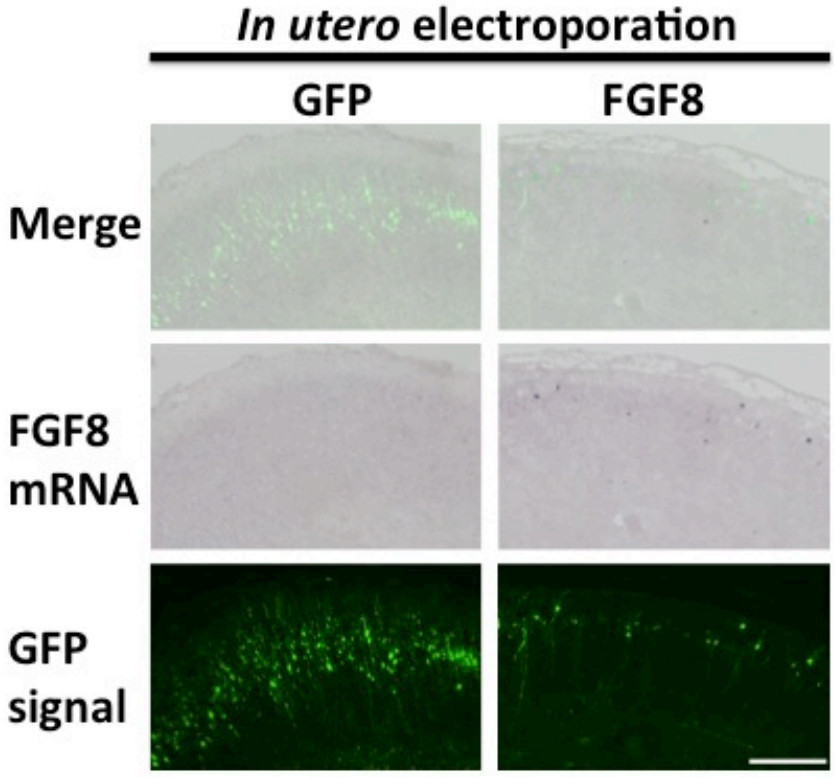

Figure 7. The distribution patterns of ectopically expressed mouse *FGF8* in the ferret cerebral cortex. After *in utero* electroporation was performed at E33, brains were prepared at P6, and coronal sections of the cerebral cortex were subjected to *in situ* hybridization with a mouse FGF8 probe. Note that mouse *FGF8* mRNA was detected in GFP-positive cells of the FGF8-transfected cortex, whereas no signals were detected in the control GFP-transfected cortex. Scale bar = 300 μm.

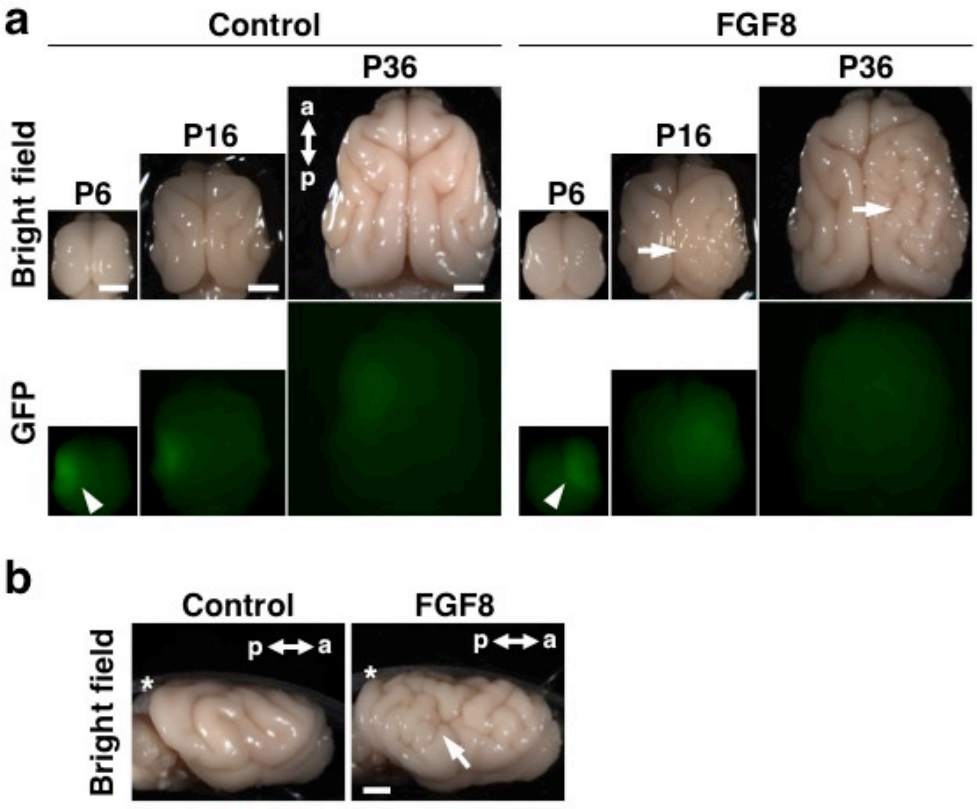

Figure 8. FGF8 induces polymicrogyria and megalencephaly in the developing ferret brain. (**a**) Dorsal views of the developing ferret brain. GFP or GFP plus FGF8 were expressed in one side of the brain at E33 using *in utero* electroporation, and the brain was prepared at the indicated time points. Electroporated areas showed GFP fluorescence (arrowheads). FGF8 induced polymicrogyria and megalencephaly at P16 and P36 (arrows). (**b**) Lateral views of the ferret brain at P36. The arrow indicates polymicrogyria. Asterisks indicate plastic dishes. a, anterior; p, posterior. Scale bars = 4 mm.

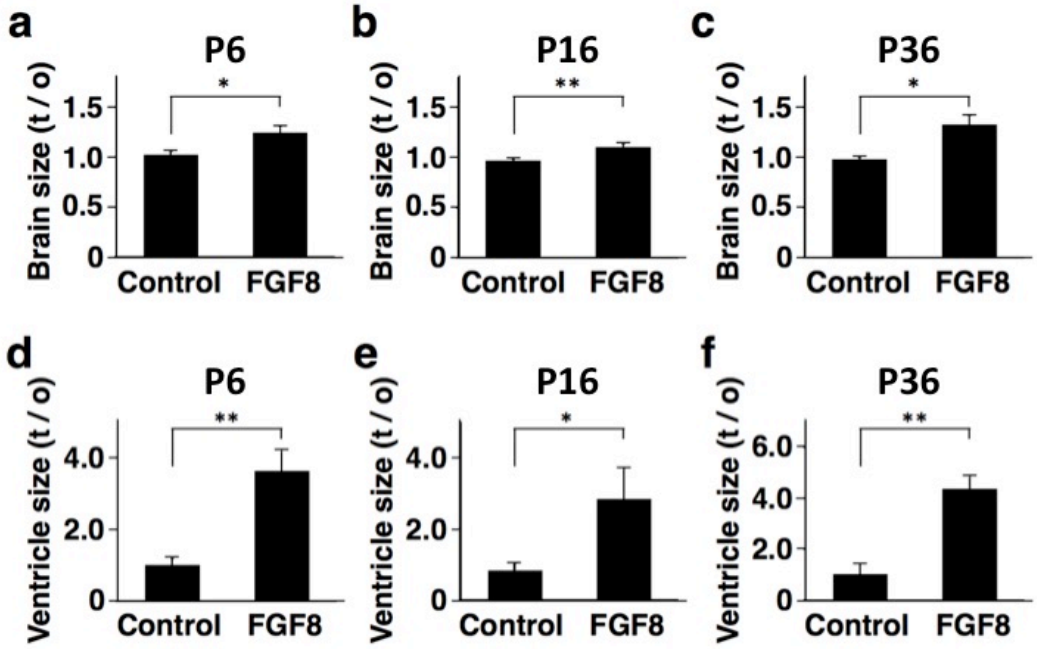

Figure 9. Quantification of the sizes of the brain and the lateral ventricle. Coronal sections containing the anterior part of the lateral ventricle were used for quantification. To minimize the variation of the size depending on the position of coronal sections, the ratio of the transfected side (t) and the other side (o) was calculated. The t/o ratio would be 1 if the size of the transfected side was the same as that of the other side, and would be larger than1 if the size of the transfected side was larger than that of the other side. (**a-c**) The brain size was significantly increased in the FGF8-transfected hemisphere than in the GFP-transfected control hemisphere. The area of the transfected hemisphere and that of the other side of the hemisphere were measured, and the ratios of these two values are shown. (**d-f**) The sizes of lateral ventricle were significantly increased in the FGF8-transfected hemisphere compared to the GFP-transfected control hemisphere. The area of the lateral ventricle of the transfected side and that of the other side were measured, and the ratios of these values are shown. Bars represent mean ± SD. *, $p<0.05$; **, $p<0.01$. n=3 for each condition.

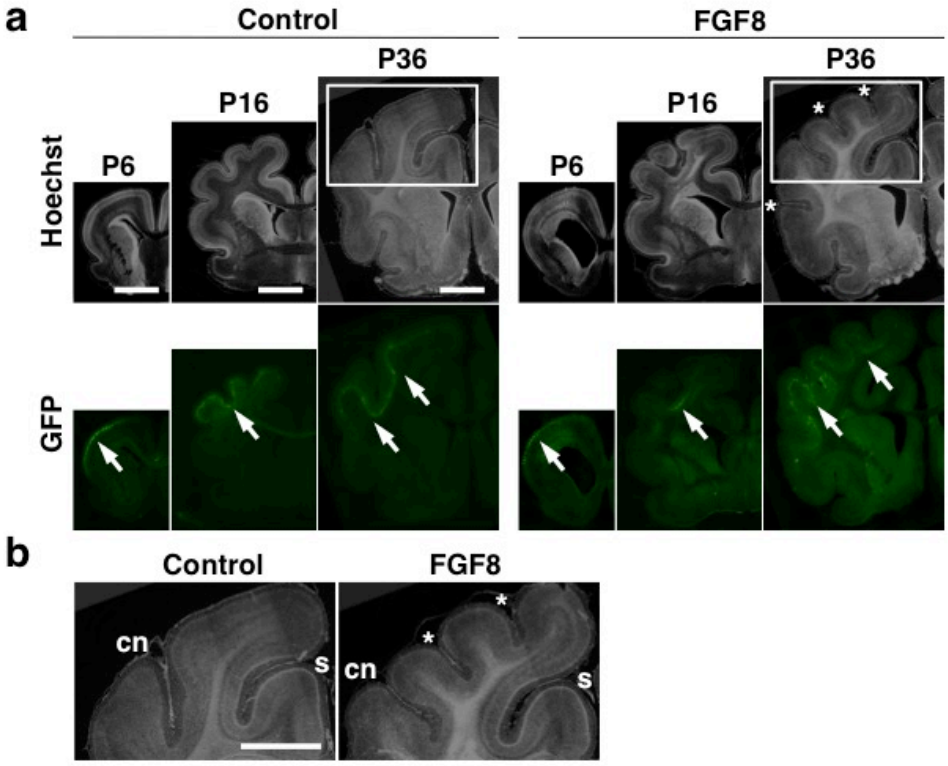

Figure 10. Histological examination of the effects of FGF8 in the developing ferret brain. (**a**) GFP and FGF8 were expressed in the ferret cerebral cortex at E33 using *in utero* electroporation, and the brain was prepared at the indicated time points. Coronal sections were prepared and stained with Hoechst 33342. Additional sulci are clearly visible at P36 (asterisks). Electroporated areas showed GFP fluorescence (arrows). Scale bars = 6 mm. (**b**) Magnified images in the white boxes in (**a**). Newly formed sulci are indicated by asterisks. s, splenial sulcus; cn, coronal sulcus. Scale bar = 6 mm.

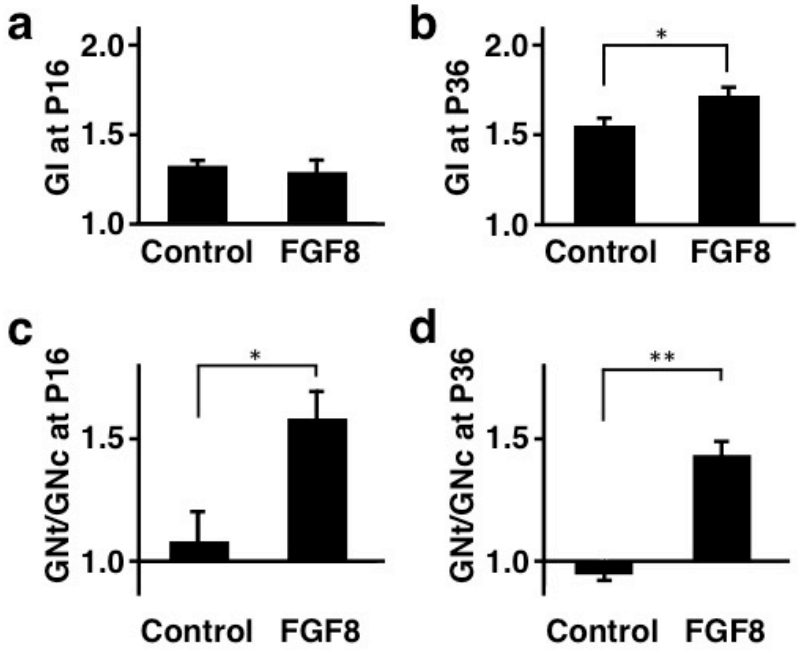

Figure 11. Quantification of the effects of FGF8 on gyrification. GFP and FGF8 were expressed in the ferret cerebral cortex at E33 using *in utero* electroporation, and the brain was prepared at the indicated time points. Coronal sections containing the anterior part of the lateral ventricle were used for quantification. (**a**,**b**) The GI values were measured using the electroporated side of the brain. The GI values were significantly larger in the FGF8-transfected brain at P36 (**b**). (**c**,**d**) The GN values were measured, and the GNt/GNo values were calculated. The GNt/GNo values were significantly larger in the FGF8-transfected brain at P16 and P36. Bars represent mean ± SD. *p<0.05; **p<0.01. n=3 for each condition.

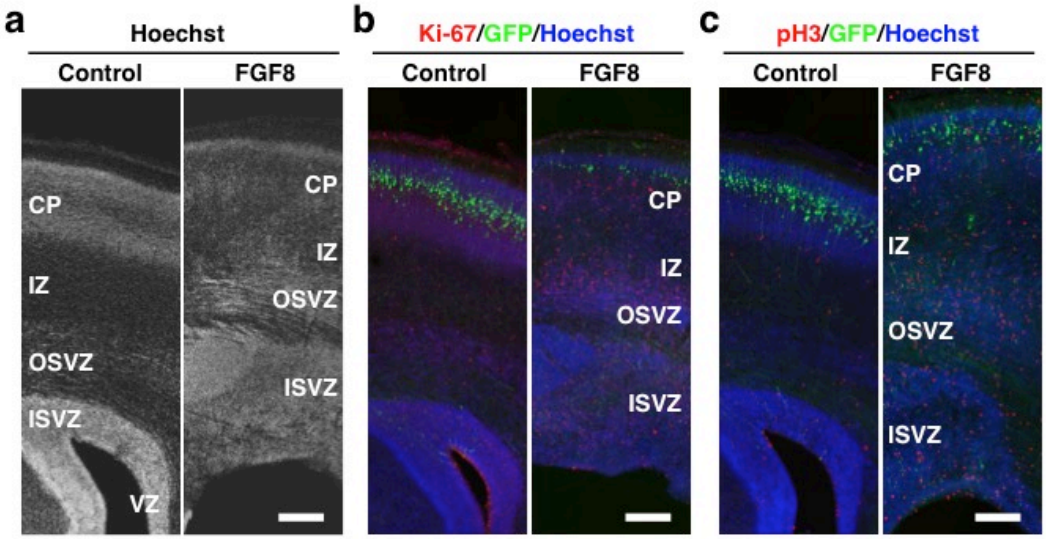

Figure 12. Cell proliferation in the cerebral cortex of developing FGF8-electroporated ferrets. GFP and FGF8 were expressed in the ferret cerebral cortex at E33 using *in utero* electroporation, and the brain was prepared at P6. Coronal sections were stained with Hoechst 33342 (white in (**a**), blue in (**b**, **c**)) plus either anti-Ki-67 antibody or anti-phospho-histone H3 antibody (red). Cortical regions containing transfected GFP-positive areas (green) are shown. Note that Ki-67-positive cells and pH3-positive cells were markedly increased in FGF8-electroporated ferrets. Scale bars = 300 μ m.

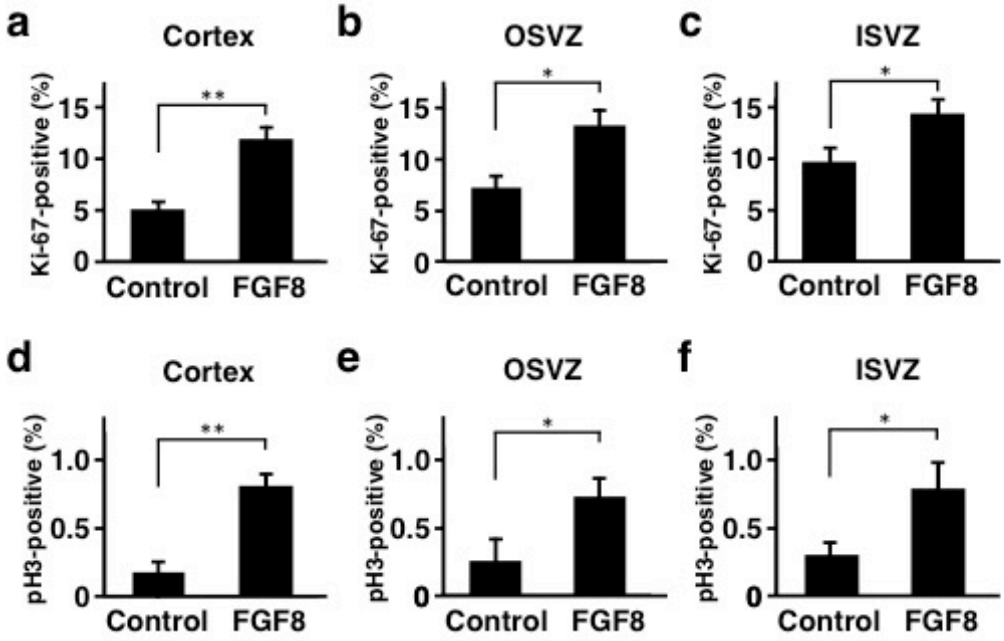

Figure 13. Quantification of cell proliferation in FGF8-electroporated ferrets. GFP and FGF8 were expressed in the ferret cerebral cortex at E33 using *in utero* electroporation, and the brain was prepared at P6. Coronal sections containing the anterior part of the lateral ventricle were used for quantification. The numbers of Ki-67-positive cells (**a**–**c**,**g**) and pH3-positive cells (**d**–**f**,**h**) were counted, and were divided by the numbers of Hoechst 33342-positive cells in the same regions. The percentages of positive cells in the cerebral cortex (**a**,**d**), the OSVZ (**b**,**e**) and the ISVZ (**c**,**f**) are shown. Bars represent mean ± SD. *p<0.05; **p<0.01. n=3 for each condition.

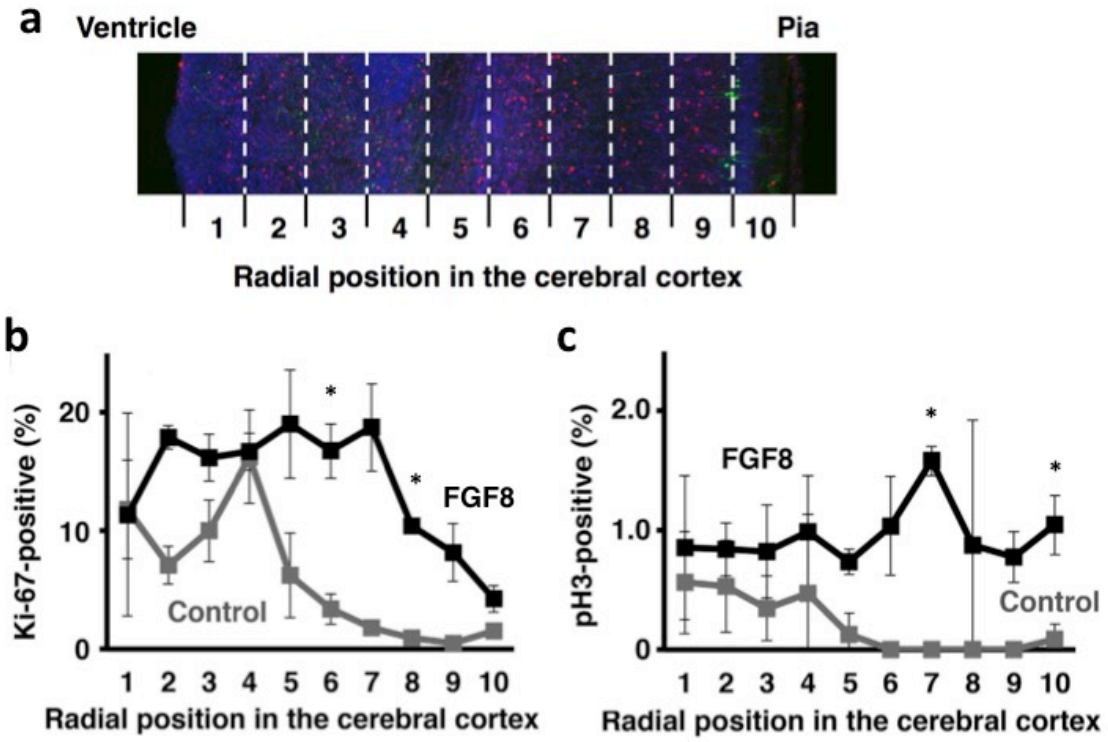

Figure 14. Quantification of cell proliferation in 10 divided regions in the cerebral cortex. (a) Images of the cerebral cortex were divided into 10 regions along the radial axis from the ventricular surface (1) to the pial surface (10). The number of positive cells (red) in each region was counted and divided by that of Hoechst 33342-positive cells (blue) in the same region. (**b,c**) The numbers of Ki-67- and pH3-positive cells in each region were counted and were divided by the numbers of Hoechst 33342-positive cells in the same region. The percentages of positive cells are shown. Bars represent mean ± SD. *$p<0.05$. n=3 for each condition.

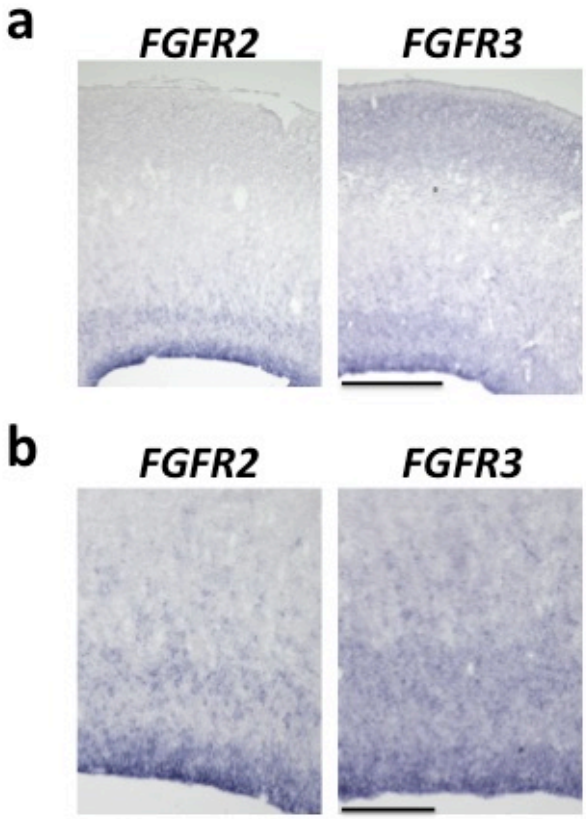

Figure 15. Expression patterns of FGF receptors in the developing ferret cortex. Expression patterns of ferret *FGFR2* and *FGFR3* mRNA in coronal sections of the ferret cerebral cortex were examined using *in situ* hybridization at E40. Note that FGF receptors were mainly expressed in the VZ and the SVZ. (**a**) Low magnification images of the cerebral cortex. (**b**) High magnification images of the VZ and the SVZ. Scale bars = 500 μm (**a**), 200 μm (**b**).

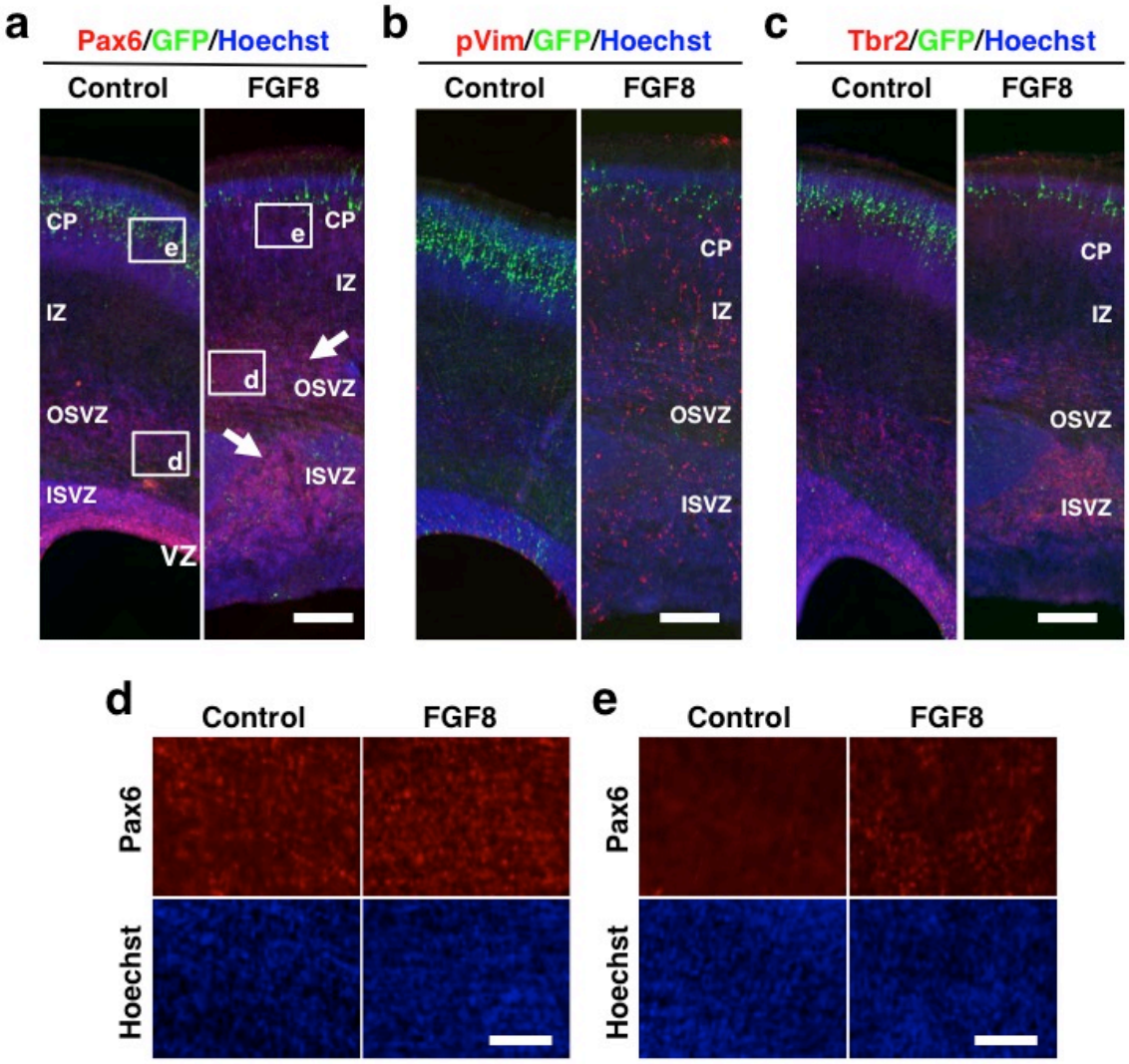

Figure 16. The distribution of Pax6-, pVim- and Tbr2-positive cells in the cerebral cortex of developing FGF8-electroporated ferrets. GFP and FGF8 were expressed in the ferret cerebral cortex at E33 using *in utero* electroporation, and the brain was prepared at P6. Coronal sections were stained with Hoechst 33342 (blue) plus either anti-Pax6 antibody, anti-phosphorylated vimentin (pVim) antibody or anti-Tbr2 antibody (red). (**a**–**c**) The cerebral cortex containing the transfected GFP-positive area (green) is shown. Note that Pax6-positive cells (arrows), pVim-positive cells and Tbr2-positive cells were markedly increased in FGF8-electroporated ferrets. (**d**) Pax6-positive cells in the OSVZ. Confocal images in the white boxes in (**a**) are shown. (**e**) Pax6-positive cells in the CP. Confocal images in the white boxes in (**a**) are shown. Note that Pax6-positive cells were markedly increased both in the OSVZ and in the CP. Scale bars = 300 μm (**a**–**c**), 100 μm (**d**,**e**).

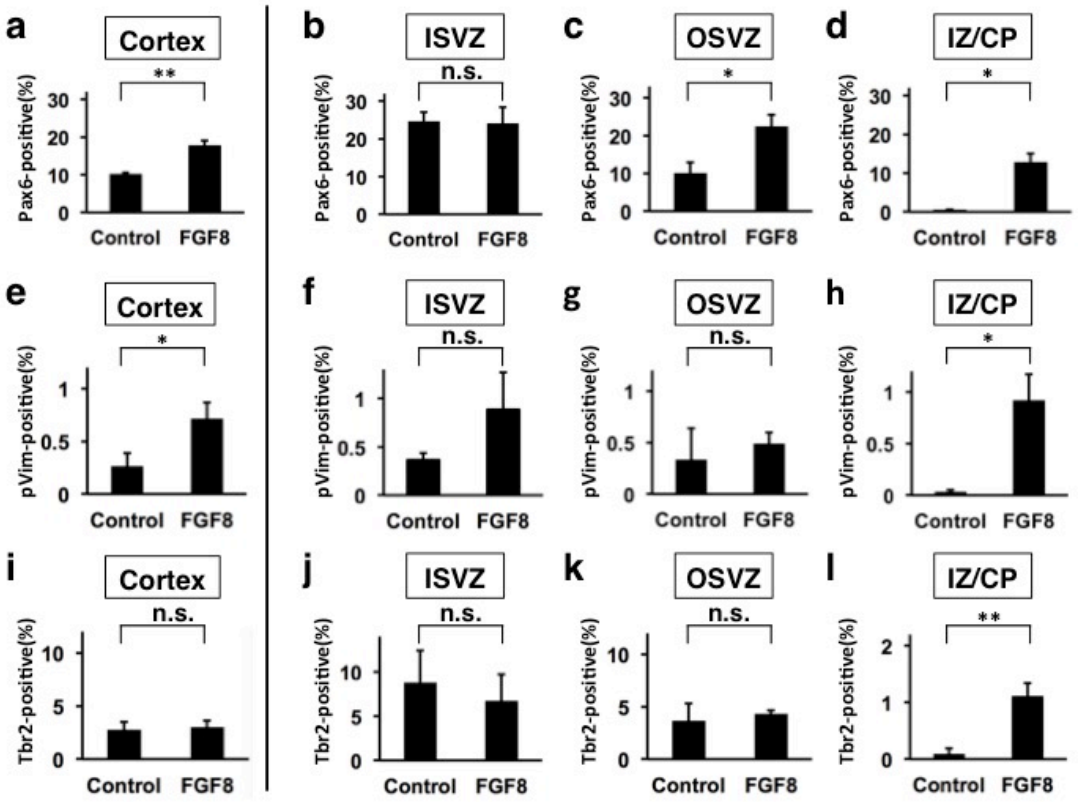

Figure 17. Quantification of Pax6-, pVim- and Tbr2-positive cells in FGF8-electroporated ferrets. GFP and FGF8 were expressed in the ferret cerebral cortex at E33 using *in utero* electroporation, and the brain was prepared at P6. Coronal sections containing the anterior part of the lateral ventricle were used for quantification. The numbers of Pax6-positive cells (**a**–**d**), pVim-positive cells (**e-h**) and Tbr2-positive cells (**i-l**) were counted, and were divided by the numbers of Hoechst 33342-positive cells in the same regions. The percentages of positive cells in the cerebral cortex (**a**,**e,i**), the ISVZ (**b**,**f,j**), the OSVZ (**c**,**g,k**) and the IZ/CP (**d,h,l**) are shown. Bars represent mean ± SD. *p<0.05; **p<0.01. n.s., not significant. n=3 for each condition.

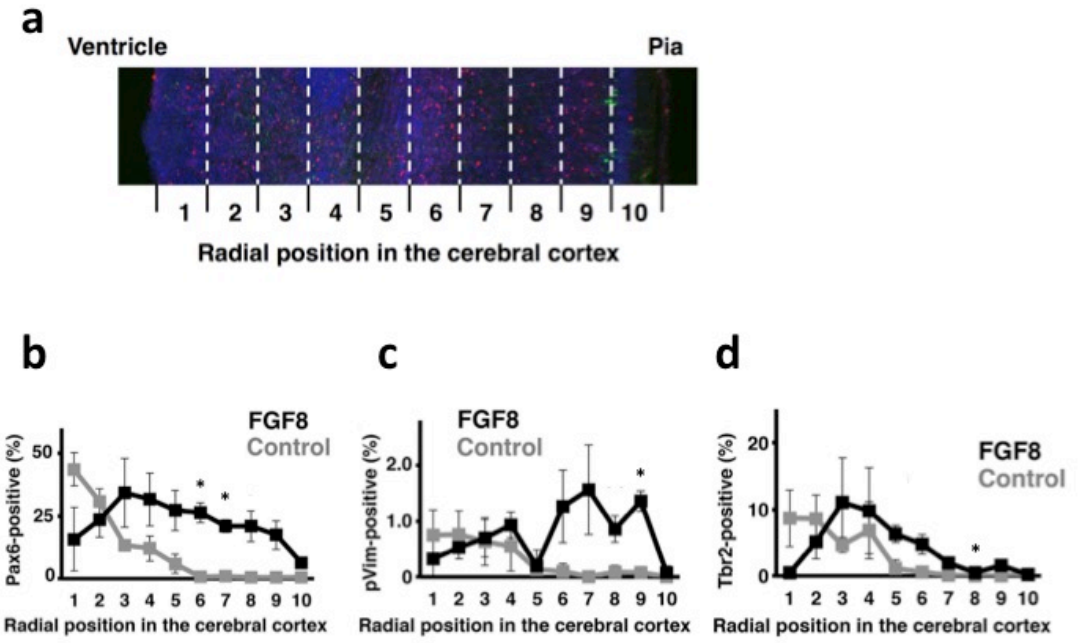

Figure 18. Quantification of Pax6-, pVim- and Tbr2-positive cells in 10 divided regions in the cerebral cortex. (a) Images of the cerebral cortex were divided into 10 regions along the radial axis from the ventricular surface (1) to the pial surface (10). The number of positive cells (red) in each region was counted and divided by that of Hoechst 33342-positive cells (blue) in the same region. (**b-d**) The numbers of Pax6-, pVim- and Tbr2-positive cells in each region were counted and were divided by the numbers of Hoechst 33342-positive cells in the same region. The percentages of positive cells are shown. Bars represent mean ± SD. *p<0.05. n=3 for each condition.

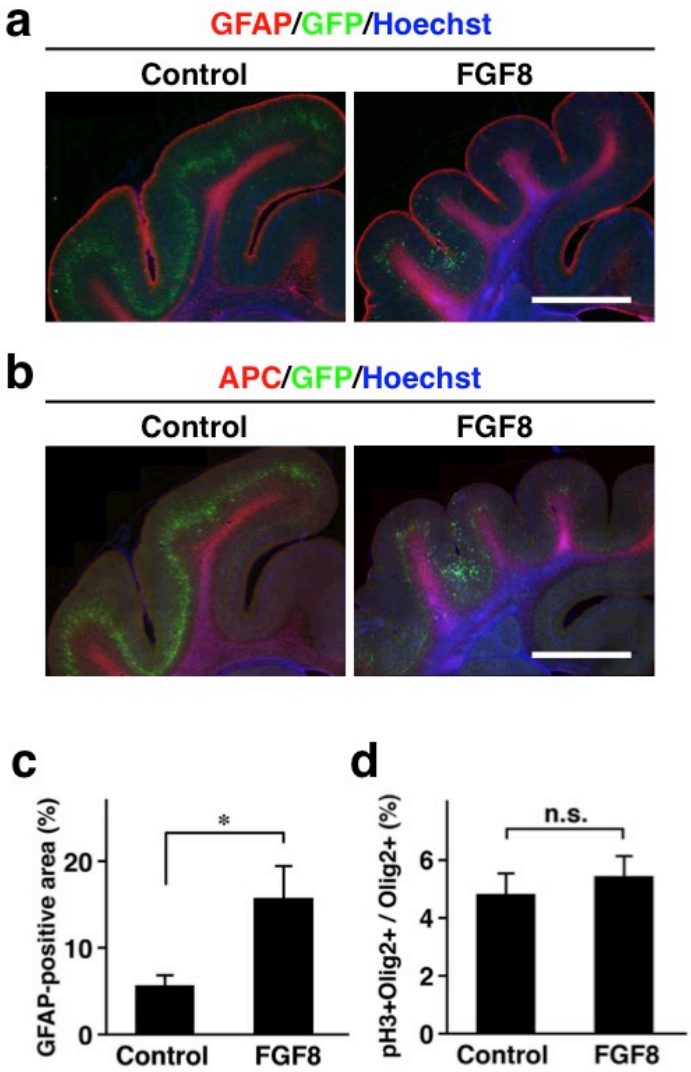

Figure 19. Astrocytes and oligodendrocytes in the cerebral cortex of FGF8-electroporated ferrets. GFP and FGF8 were expressed in the ferret cerebral cortex at E33 using *in utero* electroporation, and the brain was prepared at P6 (**d**) and P36 (**a–c**). Coronal sections were subjected to immunohistochemistry. (**a**) Sections were stained with anti-GFAP antibody (red) and Hoechst 33342 (blue). The part of the cerebral cortex containing the transfected GFP-positive area (green) is shown. (**b**) Sections were stained with anti-APC antibody (red) and Hoechst 33342 (blue). The part of the cerebral cortex containing the transfected GFP- positive area (green) is shown. (**c**) Quantification of the GFAP-positive area in the cortex. The percentage of the total area which was GFP-positive is shown. (**d**) The percentage of pH3- and Olig2-double positive cells in Olig2-positive cells. Bars represent mean ± SD. *$p<0.05$; n.s., not significant. n=3 for each condition. Scale bars = 3mm.

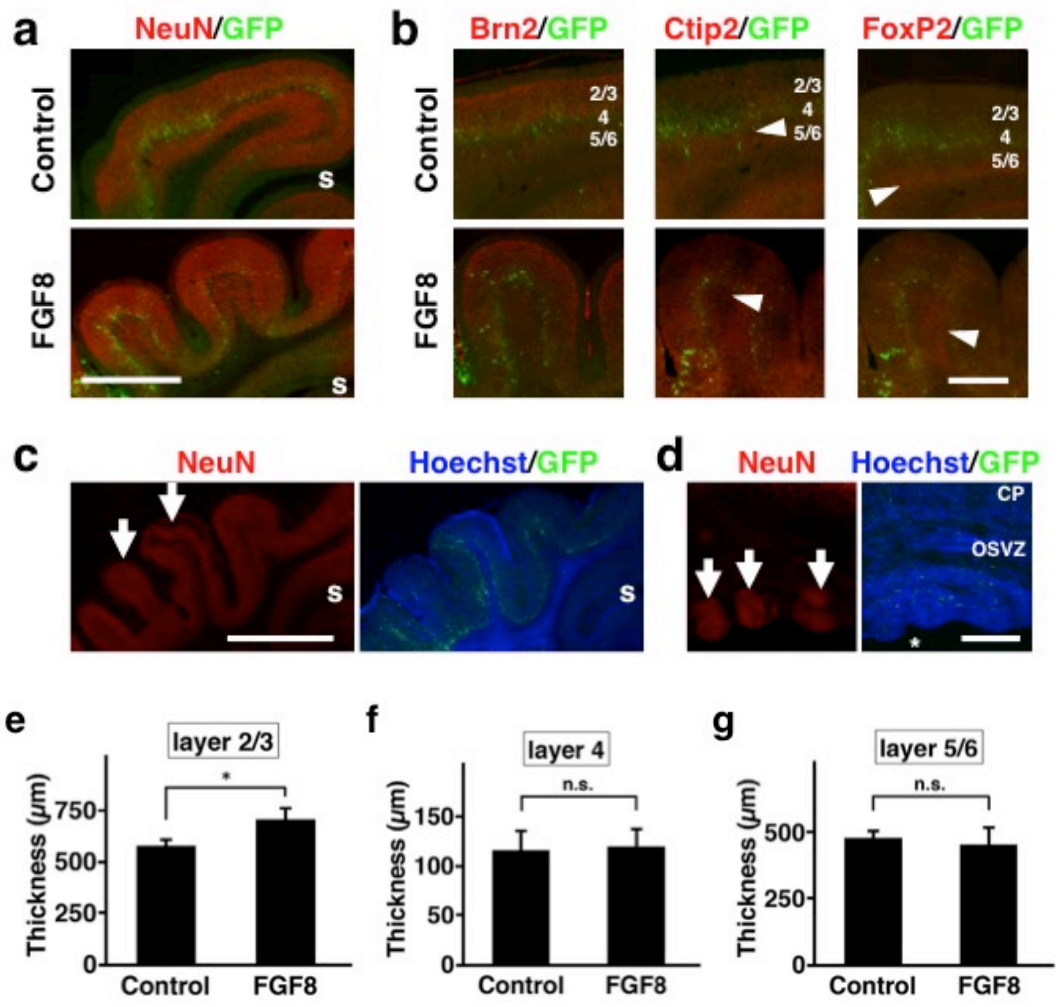

Figure 20. Layer structures in the cerebral cortex of FGF8-electroporated ferrets. GFP and FGF8 were expressed in the ferret cerebral cortex at E33 using *in utero* electroporation, and the brain was prepared at P6 (**d**) and P36 (**a-c,e,f**). Using coronal sections, immunostaining (red) and Hoechst 33342 staining (blue) were performed. GFP-positive transfected cells are shown in green. (**a**) NeuN immunostaining. Lower magnification images of the cerebral cortex of control ferrets and polymicrogyria of FGF8-electroporated ferrets are shown. s, splenial sulcus. (**b**) Higher magnification images of polymicrogyria with normal layer structures. Layer-specific expression patterns of Brn2, Ctip2 and FoxP2 were preserved in the cortical area with polymicrogyria. Arrowheads indicate immunopositive cells. Numbers indicate layers in the cortex. (**c**) Lower magnification images of polymicrogyria with distorted layer structures. Layer 2/3 neurons were predominantly increased (arrows). s, splenial sulcus. (**d**) Subependymal heterotopia (arrows). (**e–g**) The average thicknesses of layer 2/3 (**e**),

layer 4 (**f**) and layer 5/6 (**g**). Note that layer 2/3 was significantly thicker in FGF8-electroporated ferrets than in control ferrets. Bars represent mean ± SD. *p<0.05; n.s., not significant. CP, cortical plate; OSVZ, outer subventricular zone. Asterisk indicates the lateral ventricle. Scale bars = 2 mm (**a**), 1 mm (**b**), 3 mm (**c**) and 500 μm (**d**).